TAMPEREEN TEKNILLINEN YLIOPISTO
TAMPERE UNIVERSITY OF TECHNOLOGY

HEIKKI TIRKKONEN

SYNTHESIS OF NOVEL PERYLENE DIIMIDE DYE, A CANDIDATE FOR SINGLET OXYGEN PRODUCTION

Master's thesis

Inspected and approved by
Adjunct Professor,
University lecturer Alexander Efimov
20th December 2017

TIIVISTELMÄ

HEIKKI TIRKKONEN: Uuden peryleenidiimidi-väriaineen synteesi, kandidaatti singlettihapen tuotantoon
Tampereen teknillinen yliopisto
Diplomityö, 56 sivua, 4 liitesivua
joulukuu 2017
Materiaalitekniikan diplomi-insinöörin tutkinto-ohjelma
Pääaine: Materiaalikemia
Tarkastaja: Adjunct Professor, University lecturer Alexander Efimov
Ohjaaja: DI Lijo George

Avainsanat: singlettihappi, väriaine, peryleeni diimidi, reaktiivinen happi, antimikrobinen kemoterapia, valoherkistäjä

Peryleeni johdannaisilla on monia käyttökohteita fotokemiallisissa prosesseissa. Niiden käyttöä on kuitenkin vähemmän tutkittu singlettihapen tuotannossa. Eräiden peryleenidiimidien on osoitettu olevan hyviä singlettihapen tuottajia. Singlettihapella on monia käyttökohteita. Tästä syystä näiden peryleenidiimidi johdannaisten tutkiminen olisi kannattavaa.

Uusi peryleeni diimidi molekyyli syntetisoitiin käyttäen peryleeni-3,4,9,10-tetrakarboksyyli dianhydridiä lähtöaineena. Synteesi käsitti 4 askelta. Jokaisen askeleen jälkeen tuote puhdistettiin ja analysoitiin.

Analyysimenetelminä käytettiin NMR spektroskopiaa ja ESI-TOF massaspektrometriä. Lopullinen tuote analysoitiin lisäksi UV-Vis absorptio spetrometrillä.

Näitä menetelmiä yhdistämällä saatiin todennettua uusi molekyyli. Tällä aineella on keskinkertainen molaarinen vaimennuskerroin ja on järkevää seuraavaksi tutkia tämän aineen antimikrobiset ominaisuudet.

ABSTRACT

HEIKKI TIRKKONEN: Synthesis of novel perylene diimide dye, a candidate for singlet oxygen production
Tampere University of Technology
Master of Science Thesis, 56 pages, 4 Appendix pages
December 2017
Master's Degree Programme in Material Chemistry
Major: Material science
Examiner: Adjunct Professor, University lecturer Alexander Efimov
Instructor: MSc Lijo George

Keywords: singlet oxygen, dye, perylene diimide, reactive oxygen species, antimicrobial chemotherapy, photosensitizer

Perylene derivatives have many uses in various photochemical applications. Their use in singlet oxygen production has been less studied. Some perylene diimides have shown significant singlet oxygen yields. Singlet oxygen has many different uses. Therefore these perylene diimides are a lucrative field of study.

A novel perylene diimide dye was synthesized using Perylene-3,4,9,10-tetracarboxylic dianhydride as starting material. Synthesis consisted of 4 steps. After each step the product was purified and analyzed.

Analysis methods were nuclear magnetic resonance spectroscopy and electrospray ionization time-of-flight mass spectrometry. Final product was additionally characterized with ultraviolet-visible light absorption spectroscopy.

Combination of these studies enabled the verification of this novel molecule. Molecule presented moderate molar attenuation coefficient and it is viable to test the antimicrobial properties of this compound.

PREFACE

First of all I would like to thank University Lecturer Alexander “Sasha” Efimov for giving me the opportunity to work in Department of Chemistry and Bioengineering. I would also like to thank him for examining my MSc Thesis and helping me in understanding NMR spectra. Furthermore, I would like to thank my supervisor MSc Lijo Geroge for finding the time to assist me in practical and theoretical issues during my thesis. Without your efforts this thesis would not exists. I hope you excel in your future studies and receive your earned PhD.

I would like to thank the whole faculty of Chemistry and Bioengineering for creating pleasant and inspiring atmosphere. Special thanks to Anne-Maarit Tikkanen, Elina Vuorimaa-Laukkanen, Riikka Lahtinen and Marja Asp-Lehtinen for always being helpful and inspiring and Arto Hiltunen for answering my endless questions.

I’m thankful for my beloved boys for challenging me. Because of you I had the courage to return to TTY and finish my MSc degree. Johanna, my wife, I thank you for loving me as I am.

In Tampere, Finland, on 20th December 2017

Heikki Tirkkonen

CONTENTS

LIST OF FIGURES

LIST OF SYMBOLS AND ABBREVATIONS

•OH	Hydroxyl radical, oxidanyl
^1H	Proton signal
$^1\Delta_g$	Singlet excited state, lowest energy excited state
$^1\Sigma_g$	Singlet excited state, next to lowest energy excited state
$^3\Sigma_g$	Triplet ground state
5ALA	5-amino-4-oxopentanoic acid
AlPcS4	Aluminum phtalacyanine tetrasulfate
Ar	Argon gas
CC	Column chromatography
C-C	Carbon atom connected to another carbon, covalent bond
CFU	Colony forming units
COSY	Correlation spectroscopy
Da	Dalton
DMEN	N,N-dimethylethane-1,2-diamine
DMF	N,N-Dimethylformamide
ESI-TOF	Electrospray ionisation time-of-flight mass spectrometry
Ether	Diethyl ether
gHMBC	gradient selected Heteronuclear, Multiple Quantum Correlation
gHSQC	gradient selected Heteronuclear Single Quantum Correlation
h	hour
HdP	Hematoporphyrin derivate
HRMS	High-resolution mass spectrometry
Hz	Hertz, 1/second
ISC	Intersystem crossing
kcal	Kilo calories
LEU-ENK	Leucine enkephaline
$M^{-1}cm^{-1}$	Unit of molar attenuation coefficient, per mole per centimeter
MB	Methylene blue
MeI	Methylene iodide
NMR	Nuclear magnetic resonance
O_2^-	Superoxide anion, dioxide (1-)
PACT	Photodynamic antimicrobial chemotherapy
Pc	Phtalocyanine
PDI	Perylene diimide
PDT	Photodynamic therapy
PpIX	Protoporphyrin IX
ppm	Parts per million
PS	Photosensitizer
PTCDA	Perylene-3,4,9,10-tetracarboxylic dianhydride
Qt-	Quaternary
RB	Rose Bengal
R-H	Compound that contains hydrogen
ROS	Reactive oxygen species
RT	Room temperature, around 22 °C
S	Total spin number
TBO	Toluidine blue O
TLC	Thin layer chromatography

TMS	Trimethylsilane
m/z	charge per mass
Å	Ångström, 10-10 m
µm	1´10-6 m
Φ_{Δ}	Singlet oxygen quantum yield

1. INTRODUCTION

At the beginning of 21st century, one of the most crucial health care issues in the world is antibiotic resistance. While increasing number of pathogenic bacteria are developing resistance against antibiotics, the amount of new antimicrobial drugs is decreasing every year. Antibiotics work by single mode or action and given enough time bacteria are able to develop sufficient countermeasures against them.

A novel approach is to use excited oxygen molecules to inflict damage to microbes. These reactive oxygen species are naturally occurring *in vivo* and most of them are tolerated by cells to some extent. Singlet oxygen is the most reactive of these species and human pathogenic bacteria have no counter mechanisms against it.

This approach is utilized in photodynamic antimicrobial chemotherapy. It is a treatment, which applies photosensitizers, a light source and oxygen from air. Unfortunately this type of treatment can only be applied topically, as tissue absorbs light very effectively. Suitable areas include: skin, lungs, nasal- and abdomen cavities.

Similar approach could be applied to create antimicrobial surfaces. This could be achieved by surface coating, which would incorporate the photosensitizers. These surfaces could be applied wherever there is sufficient lighting. These antimicrobial surfaces could decrease the need of antibiotics altogether.

Already several different types of photosensitizers have been developed. They are divided in to several groups according to their general molecular structure. They all have similar attributes, which include: decent absorption of visible light, good singlet oxygen yield and high molar attenuation coefficient.

Perylene derivatives have been less explored as antimicrobial photosensitizers. However, they possess many desirable qualities and are therefore viable candidates for further investigation.

In this work one novel perylene diimide derivate was synthesized. The structure of the molecule was verified by mass spectrometry and nuclear magnetic resonance spectroscopy.

Future studies include the verification of singlet oxygen quantum yield, dark toxicity and antibiotic properties of this novel molecule. Furthermore this molecule could be applied in tandem of suitable coating material to create antimicrobial surfaces. This molecule

could be used as basis of derivatives that could be applied as antimicrobial agents in photodynamic antimicrobial chemotherapy.

2. LITERATURE REVIEW

This review first takes a look at photodynamic antimicrobial chemotherapy. This is one of the main motivations behind this novel dye. The mechanism of action is the use of reactive oxygen species and singlet oxygen in particular. Singlet oxygen is also used in photodynamic therapy, which has the same principle of action that is used in photodynamic antimicrobial chemotherapy applications. Common photosensitizer dyes are introduced and finally the use of perylene derivatives as photosensitizers is explained.

2.1 Introduction to photodynamic antimicrobial chemotherapy

Dye therapy, without the use of photoactivation, has been used in the early 19th century to kill bacteria. One example is the use of methylene blue as a cure for malaria in 1891. After the discovery of penicillin, the research efforts switched from dyes to antibiotics derived from natural products, such as yeasts. However, they have an inherit problem: conventional antimicrobial drugs work with single mode or action. This enables microbes to develop resistances against them after sufficient exposure. [1]

Some bacteria many form protective biofilm that is resistant to antibiotics and biocides. Biofilm protected bacteria need at least an order of magnitude higher concentration of these antibacterial agents in order to be killed as opposed to bacteria that are unprotected by biofilm. An example of biofilm in humans is dental plaque. [2]

Nowadays several antibiotic resistant human pathogenic bacteria are known and effective means are needed as bacterial infections are once more becoming untreatable. In addition the number of new antibacterial agents approved for medicinal use is declining every year. One such approach is to apply photosensitizers in photodynamic antimicrobial chemotherapy (PACT). [3], [4]

This is a form of antimicrobial therapy that utilizes the use of photosensitizer (PS), oxygen and light. Currently PACT is used in skin pathogen decolonization, burn wound disinfection and treating oral cavity infections, such as root canal infection. [4]

2.2 Reactive oxygen species

PACT relies on *in situ* production of reactive oxygen species (ROS). These are usually created by radical reactions or by energizing molecular oxygen. ROS include: superoxide (O_2^-), hydrogen peroxide (H_2O_2), hydroxyl radical (•OH) and singlet oxygen ($^1\Delta_g\ O_2$). The first two are well tolerated in low levels by micro-organisms as they are produced in aerobic metabolism and respiration. Organisms are poorly capable to defend against hy-

droxyl radicals and singlet oxygen and additionally large amounts of superoxide or hydrogen peroxide may defeat the defense mechanisms that micro-organisms have against these ROS. Singlet oxygen is considered to be the most effective ROS against living organisms. In addition human pathogenic bacteria seem to have no singlet oxygen quenching strategies. This makes PACT a viable option as antimicrobial method and singlet oxygen the most interesting of all ROS. In PACT singlet oxygen is generated by energy transfer from excited PS molecule to molecular oxygen. [5], [6]

2.2.1 Excited state of molecular oxygen

Oxygen is present in atmosphere and it is usually in molecular (O_2) form that consists of two oxygen atoms. Atmosphere contains around 0.209 mole fractions of O_2 at sea level. [7, p. 176] Oxygen atom has 8 electrons and their distribution in orbitals can be observed in Figure 1 below, which represents the electronic configurations of ground and excited state oxygen molecules. Electronic configurations follow Hund's rule: "*The lowest-energy configuration for an atom is the one having the maximum number of unpaired electrons allowed by the Pauli principle in a particular set of degenerate orbitals.*" [7, p. 562] Pauli's principle states, that "*An orbital can hold only two electrons, and they must have opposite spins.*" [7, p. 556] Oxygen molecule has completely filled bonding 2pσ and 2pπ orbitals and it has two unpaired electrons in anti-bonding 2pπ orbital.

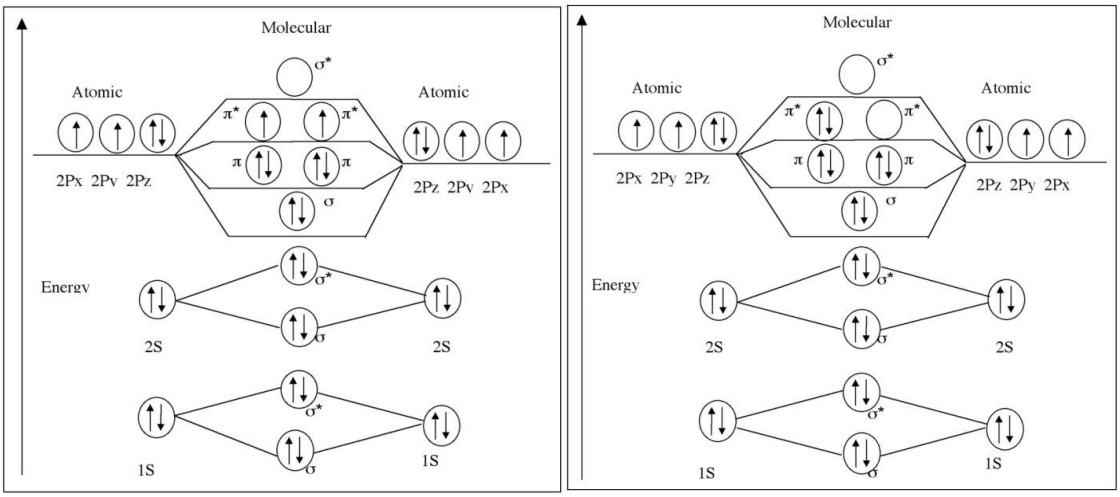

***Figure 1**. Electronic configurations of triplet (left) and singlet (right) molecular oxygen.* **[8]**

Electrons have elemental quantum chemical property called spin. It has two possible values up or +½ and down -½. Nearly all organic molecules contain even number of electrons. Additionally these electrons have equal number of up and down values. [9, p. 14561] Spin states of molecules can be defined with the use of spin multiplicity:

$$2S + 1, \qquad (1)$$

Where *S* is the total spin quantum number. For these organic molecules the total spin number (*S*) gets the value of 0 and the multiplicity gets the value of 1. They are therefore said to have singlet state.

Molecular oxygen on the other hand has two more electrons with one spin state than the other in its ground state. This is presented in left diagram in Figure 1 above. Furthermore because of these unpaired electrons, it has a permanent magnetic moment and it has total spin number of 1 in its ground state and the multiplicity gets value of 3. It is therefore said to have triplet ground state ($^3\Sigma_g$). [10] Triplet ground state is the most stable and abundant form of oxygen, but it is possible to excite O_2 to singlet excited state ($^1\Delta_g$) with sufficient amount of energy. [8]

Transformation from $^3\Sigma_g$ to $^1\Delta_g$ state is spin-forbidden and because of this triplet ground state oxygen is relatively poor oxidizer for organic molecules under normal reaction conditions. For example the reaction rates for oxidation reaction of linoleic acid are 1.3×10^5 M^{-1} S^{-1} and 8.9×10^1 M^{-1} S^{-1} for $^1\Delta_g$ oxygen and $^3\Sigma_g$ oxygen respectively. [8]

2.2.2 Singlet oxygen production through photodynamic effect

Oxygen molecule can be excited and it has two excited states with relatively low excitation energies. These states are presented in Figure 2 below. The transition from first excited singlet state ($^1\Delta_g$) of O_2 to the triplet state $^3\Sigma_g$ is spin forbidden, therefore singlet excited state $^1\Delta_g$ is relatively long living. However, singlet oxygen is extremely reactive, which limits its effective radius in practical applications. This radius is dependent on the mean diffusion path length, which $^1\Delta_g$ can take before it gets in contact with reactant. Transition from second excited state ($^1\Sigma_g$) is not spin forbidden and therefore this species is readily relaxed to $^1\Delta_g$. Although the electronic configuration in the second excited state is similar to ground state, the last two electrons have antiparallel spins. [11][12]

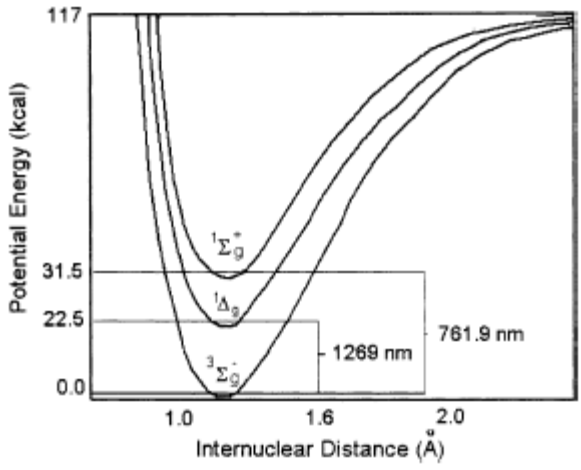

Figure 2. *Potential energy (kcal) per internuclear distance (Å) for molecular oxygen.* **[11]**

There are several ways to produce singlet oxygen. These include enzymatic, chemical and photochemical routes. This thesis will concentrate on the photochemical route. This method involves photosensitizers that are molecules witch can absorb and transfer energy to oxygen molecule in order to excite it to singlet state. This process of excitation is described with Jablonski diagram in Figure 3 below. [8]

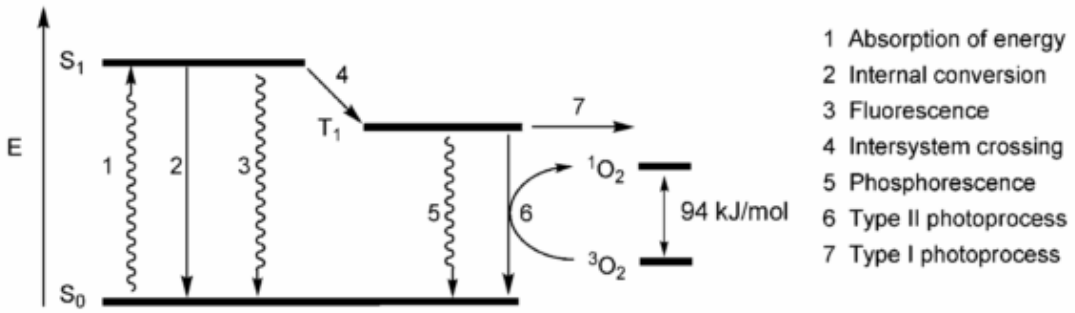

***Figure 3**. Jablonski diagram explanation on working of photosensitizers.* **[13, p. 4]**

Photosensitizers need to have: high absorption coefficient with the spectral region of used light, triplet state of the PS needs to have at least 94 kJ mol^{-1} of energy above ground state and to have a relatively long lifetime in order for them to work efficiently as photosensitizers. The process of photoexcitation is described in Equation 2 below. [11]

$$P(S_0) \overset{h\nu}{\rightarrow} P(S_1) \overset{k_{ISC}}{\longrightarrow} P(T_1) \tag{2}$$

In the above equation P is photosensitizer, S_0 is singlet ground state, S_1 is first excited singlet state, T_1 is first excited triplet state, $h\nu$ is process of photoexcitation and k_{ISC} is the reaction rate of intersystem crossing.

In the excitation process PS are excited with light that has suitable wavelength. This excites PS from ground state S_0 to short lived lowest excited singlet state S_1. Lifetime of this S_1 state is in the nanosecond range. From here relaxation can happen through internal conversion, fluorescence and intersystem crossing (ISC). Singlet oxygen production happen via two photoprocesses that are indicated in Figure 3 as Type I and Type II. Therefore, the ISC is the most important pathway of S_1 relaxation for photosensitizers. [13, p. 4]

In internal conversion the excited state is relaxed via heat emission and in fluorescence the relaxation happens with the release of photon. Excited singlet state S_1 can also relax to excited triplet state via intersystem crossing. Even though ISC is spin-forbidden pathway a good PS will readily undergo this process. Because of the spin-forbidden nature of this reaction, the excited triplet state is relatively long lived. [8]

Intersystem crossing reactions can happen via Type I or Type II pathways that are competitive. In Type I pathway the excited PS will react directly with compound containing hydrogen (R-H). This reaction will happen either by donating or accepting hydrogen or

electron. This will form a radical that will react further. These radicals will produce compounds such as hydrogen peroxide, anionic superoxide, hydroxyl radicals, nitric oxide and peroxide nitrite. In Type II pathway the PS will react with molecular oxygen O_2 ($^3\Sigma_g$) and excite it to singlet state O_2 ($^1\Delta_g$). Singlet oxygen is one of the reactive oxygen species. This singlet oxygen can further react as electrophile. The rate of Type II pathway reaction depends mostly on the oxygen concentration and its solubility in the system as over 99 % of the reactions between triplet PS and triplet O_2 form singlet oxygen. If the system runs out of oxygen the pathway may shift from Type II to Type I. [8][14]

Singlet oxygen quantum yield (Φ_Δ) is the efficacy of PS to produce singlet oxygen through Type II pathway of relaxation presented in Jablonski diagram above. This is a comparable number for different singlet oxygen producing photosensitizers that tells how efficiently the excitation of PS leads to singlet oxygen production. [15]

Φ_Δ of substance X is calculated using oxygen uptake experiment data and comparing this to a standard.

$$\Phi_\Delta^X = \Phi_\Delta^{Std}\left(\frac{R_{O_2}^X}{R_{O_2}^{Std}}\right)\left(\frac{I^{Std}}{I^X}\right) \quad (3)$$

Where $\Phi_\Delta{}^{Std}$ is the singlet oxygen quantum yield of the standard, R_{O_2} is the initial rate of oxygen uptake and I is the integrated absorption spectrum over the transmission range of the filter that is used to normalize the number of photons absorbed by the sample and standard. [16]

2.2.3 Applications for singlet oxygen and other ROS

Singlet oxygen is notably more electrophilic than ground state oxygen, being ca. 1 V stronger oxidant. [11] It will react readily with unsaturated carbon-carbon (C-C) bonds, anions and neutral nucleophiles including sulfides and amines. Therefore, it can be utilized in organic chemistry as synthetic reagent. [11], [17], [18]

In synthesis singlet oxygen is generally reacted with olefin by 1,4-cycloaddition, “ene” reaction or 1,2-cycloaddition. These result in endoperoxide, allylic hydroperoxide and dioxetane respectively. The stereochemistry and the structure of the resulting molecule can be adjusted selecting different solvent and reaction systems. [17]

Singlet oxygen has been utilized in photodynamic therapy (PDT). In PDT photosensitizers are excited with light that passes human tissue while still having enough energy to excite oxygen to singlet state. However, for efficient singlet oxygen production the energy of the PS triplet state should be somewhat higher than 94 kJ mol^{-1}. This limits the optimal wavelengths between 680 nm and 800 nm. Human tissue filters out shorter wavelengths and longer wavelengths do not have enough energy to efficiently excite singlet oxygen. Ideal photosensitizers would have these characteristics: availability, synthesizability,

high singlet oxygen quantum yield, strong absorption in 680-800 nm region with high attenuation coefficient, effective accumulation in tumor tissue and low dark toxicity for PS and its metabolites, Stable and soluble to tissue fluids and fast excretion from the body after treatment.[13, p. 34] Furthermore it should not be toxic without photo activation and it should have short enough half-life in patient to reduce the unwanted effects, such as light sensitivity. This mechanism of action is the same that is used in PACT. However, in PACT the targets are microbes instead of cancer cells.

In PTD of cancer the photosensitizer is administered to patient. PS will then accumulate in the tumor during drug-light interval. Light is then administered directly to tumor using suitable wavelength. This can be achieved via regular lamp but usually fiber optics and laser is used. PS will produce the cytotoxic products from oxygen (Type I or Type II pathway) and these will destroy the tumor while leaving healthy tissue unharmed. [19]

2.3 Applications of PACT

Bacteria have multiple strategies to counter oxidative stress. Superoxide dismutase, peroxidase and catalase are enzymes that neutralize the toxicity of ROS and protect bacteria from its environment. In addition in photosynthetic bacteria singlet oxygen can be quenched by triplet state of chlorophyll during photosynthesis or quencher molecules like carotenoid. [20] The main drawback in PACT compared to antibiotic is that PACT can currently only be applied topically. This limits the use of PACT to surface layers of different orifices and skin. This is due the fact that PACT requires photoactivation and the intensity of light will drastically decrease while travelling in tissue. [6]

Most bacteria can be divided in to two groups using Gram staining. This test gives either positive or negative value depending on the chemical and physical properties of their cell walls. Gram (+) species have porous outer wall that allows PS with molecular weight up to 30000-60000 Da to cross, while Gram (-) species have outer membrane that prevents PS from entering bacteria unless their molecular weight is lower than 600-700 Da and PS is hydrophilic. Therefore Gram (-) bacteria are less sensitive to PACT. To circumvent this PS used in PACT should be cationic and hydrophilic so it can attach to Gram (-) bacteria outer wall. [6]

So far the use of photoactivated dyes in antimicrobial treatment has been at experimental level and they are applied ancillary to conventional antimicrobial chemotherapy. Main issues in larger implementation of PACT instead of antibiotics are due to the clinical nature of the treatment, physical properties of the dye itself and the difficulty in administration. PACT treatment needs to be given in clinical environment as it includes drug administration, drug-light interval, illumination and removing of dye. Compared to antibiotic treatment, this is much more time consuming and cannot be done by patient at home. The dye itself is visible, coloring agent that will induce coloration on applied tissue. This is a minor issue when decision is between coloration of skin and death of a

patient, but again when compared to non-coloring antibiotics PACT is less desirable. Currently PACT cannot be applied against large systemic infections such as septicemia. However, infections could be treated by PACT before they spread throughout the whole body. [1]

Photosensitizers do not need to be in direct contact with bacteria for them to be effective. If PS is relatively close to bacteria the generated ROS can still have effect on nearby bacteria. This can be achieved by incorporating PS to surface that is in contact with bacteria. Compared to antimicrobial effect of PACT this method is far less efficient. However, this method allows continuous illumination of the PS and generation of ROS. Therefore the antimicrobial effect becomes sufficient. [21] This opens up several possibilities to use the photodynamic effect against. Additionally this would allow full removal of PS from treated tissue when used in PACT.

Another approach is to reduce the number of pathogens around us. One significant source of pathogens is contaminated environment. [22], [23] This issue could be addressed with antimicrobial surfaces. Pathogens could be disinfected on surfaces using photosensitizers, oxygen from air and light from common light bulbs. Additionally when PSs are used outside of human body the suitable absorption range is not restricted to 680 nm, but can include shorter wavelengths. By creating antimicrobial surfaces the need for antibiotics in general would decline. In addition to all surface materials used in hospitals, antimicrobial surfaces could be employed for example in mass transit systems and surface materials in public restrooms. The need for such surfaces is greatest in areas that are used by large masses or by already weakened individuals. [24]

2.4 Immobilization of photosensitizers

Photosensitizers could be implemented into surface materials either by encapsulating the dye molecules into the surface or by bonding the dye molecule to surface. However, this bonding should be strong enough to prevent leeching of dye out of the surface. Additionally the PS needs to be in close proximity of the bacteria.

Several different photosensitizers have been immobilized onto natural and synthetic polymers. These PS are introduced in the next chapter. Matrices for immobilization include: nanotubes and silica beads; synthetic polymers like polystyrene, polyurethane and nylon as well as natural polymers like chitosan, cellulose and cotton. Simplest method, where dye is dissolved, solution is applied directly on to surface and solvent is let to evaporate, would not sufficiently attach dye on to surface. Leeching of PS is a frequently encountered issue which can potentially lead to discharge of hazardous agents from the matrix. Therefore effective means of immobilization are required.

One example of encapsulation is “swell-encapsulation-shrink” method. In this method crosslinked polymer is put in to appropriate solvent system that will allow the polymer to

swell. This will enable the dye and other small particles, such as nanoparticles, to enter the polymer matrix. After the solvent is removed by drying the polymer will shrink back to its original size. This could be used for silicone and polyurethane which are used in urinary catheter devices. This method was used to incorporate gold nanoparticles with phenothiazinium dyes (Methylene Blue and Toluidine Blue O) into aforementioned polymers. After illumination with 660 nm low power laser it was found that mechanical properties of these dyed polymers were not affected negatively. This material proved to be effective against both gram (-) and gram (+) bacteria with laser illumination. [24], [25]

Dye molecules can be attached to polymer structure with ionic bonds. However, this could adversely affect the singlet oxygen quantum yields. This effect was presented in study by Inbaraj et al. [26] as they bonded cationic porphyrin derivatives onto functionalized polystyrene beads.

Dye molecules can also be covalently bonded to surface. This is advantageous as the dye will come to closer contact with the bacteria, while still being strongly bonded to the surface. Phenothiazinium dyes were covalently bonded on to silicone rubber polymer. Despite the very small amount of dye present in silicone surface the samples demonstrated significant antimicrobial activity under illumination. [27]

Another example of covalent bonding is nylon fiber which had protoporphyrin IX and zinc protoporphyrin IX covalently bonded to it using poly(acrylic acid) scaffold. This scaffold was used to increase the number of reactive sites on nylon-6,6 fibers for which the photosensitizer molecules could attach. This modified nylon-6,6 fiber showed antimicrobial properties against gram (+) bacteria under illumination. Light intensity used in these tests was from 10 000-60 000 lux. This was partially above normal room light, which is around 30 000 lux. The zinc protoporphyrin IX version proved to be more efficient in killing gram (+) bacteria. However the efficacy of bacteria killing was under 2 log difference in colony forming units (CFU) throughout the test setup. [28], [29]

Covalent bonding seems to be the best available option to prevent the leeching of dye molecules. This is the strongest bonding available for dye molecules.

2.5 Traditional photosensitizer dyes

Reactive oxygen species can be generated by several different photosensitizer molecules. These are molecules that absorb light in wavelengths that cover the visible light spectrum These molecules are often used in everyday life as colorants because of this ability to absorb and reflect visible light. These dyes can be divided to different groups by their core structures.

2.5.1 Porphyrins

Porphyrin is the core for many derivatives that have been accepted as candidates for PDT. These include: Photofrin® (**5**) (hematoporphyrin derivative), Levulan® (5-aminolevulinic acid, **14**), Metvix® (methyl aminolevulinate) and Visudyne® (verteporfin). In this list Levulan® and Metvix® are prodrugs that transform into porphyrin derivatives via enzyme activity. These are presented more in depth later. [30]

Porphyrin derivatives absorb light at long wavelengths very efficiently. This increases their efficacy in PDT. Extinction at longer wavelengths is stronger with chlorin and bacteriochlorin. In addition, coordinated metal in the center of molecule can blue shift the furthest red absorption band and it strengthens the most bacteriochlorin bands. [31]

The porphyrin, chlorin and bacteriochlorin molecules are presented in Figure 4 below. Chlorin has a double bond in pyrrole ring B reduced (positions 7,8). Bacteriochlorin has two bonds reduced in rings B and D (positions 7,8 and 17,18 respectively). These differences have been emphasized using circles in below Figure 4. [19]

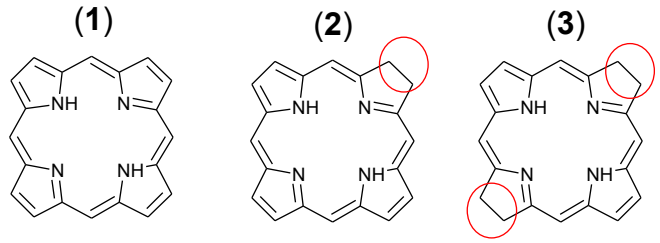

Figure 4. *Molecules of porphyrin (**1**), chlorin (**2**) and bacteriochlorin (**3**) respectably. Difference between the molecules has been emphasized using circles.*

The first United States Food and Drug administration approved PDT sensitizer for cancer treatment belonged to porphyrin family, being a hematoporphyrin derivate (HpD). It was porfimer sodium that was sold under the brand name Photofrin®(**5**). Porphyrin family also includes hemoglobins that are porphyrin derivates containing iron. One example, Heme B, can be seen in Figure 5 below. Hematoporphyrin, the first candidate for PDT, was first produced by removing the iron from blood pigment hemin.[19]

(**4**)

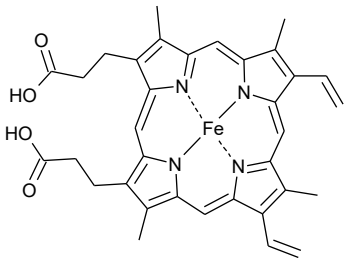

Figure 5. *Molecule of Heme B (**4**).*

Photofrin® belongs to first generation of photosensitizers. They are a group of PS that have mixture of different mono-, di- and oligomeric porphyrin structures and their molar attenuation coefficient (ε_{max}) is relatively low. For Photofrin® the wavelength for maximum absorption (λ_{max}) is at 630 nm with ε_{max} value around 3000 M^{-1} cm^{-1}. [19] This wavelength is not optimal, as tissue penetration at 630 nm is around 2-3 mm. Furthermore Photofrin® accumulates in tissue and results in photosensitivity for 6 to 10 weeks. On the positive side its singlet oxygen quantum yield is high, Φ_{Δ}=0.89. Photofrin® has been approved for PDT treatment of several different types of cancer that affect some tissue surface. These include endobroncheal, cervical, lung and bladder cancers. [19]

(**5**)

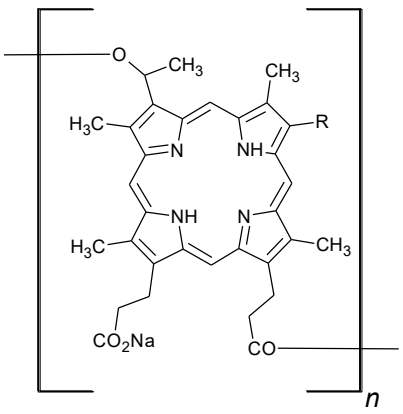

Figure 6. *Structure of Photofrin (**5**), where n=0..6*

Second generation of photosensitizers were more potent in PDT than HpD, but still presented significant undesirable photosensitivity after treatment. One example of these is meta-tetra(hydroxyphenyl)porphyrin (m-THPP) as seen in Figure 7 below.[19] This constitutes of porphyrin skeleton that has 4 meta-hydroxyphenyl substituents attached to it. Substance m-THPP has λ_{max} value of 644 and ε_{max} value of 3400 with Φ_{Δ} being 0.61 in air saturated solution. [32], [33]

(**6**)

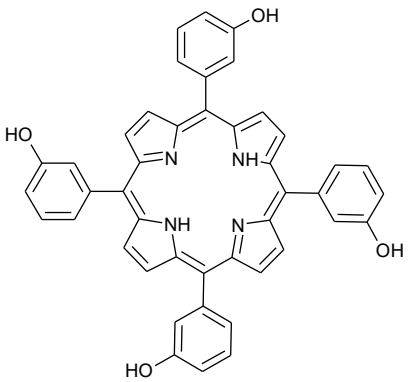

Figure 7. *Example of second generation photosensitizers, m-THPP (**6**).*

Several candidates for PDT are derived from chlorin family. Chlorin based PDT drugs include: Foscan® (Temoporfin), Laserphyrin® (Talaporfin) and Photochlor® (HPPH). [30] Chlorins differ structurally from porphyrins only by having the *C* pyrrole ring reduced at 17,18-positions. Molecule in Figure 8 below is meta-tetra(hydroxyphenyl)chlorin, (m-THPC, **7**). The difference between chlorin and porphyrin is emphasized with red circle in structure on m-THPC. This small difference in structure shifts absorption band from 640 nm to 700 nm. m-THPC is sold under brand name Foscan® and it has ε_{max} of 29600 M^{-1} cm^{-1} at 650 nm. [19]

(**7**)

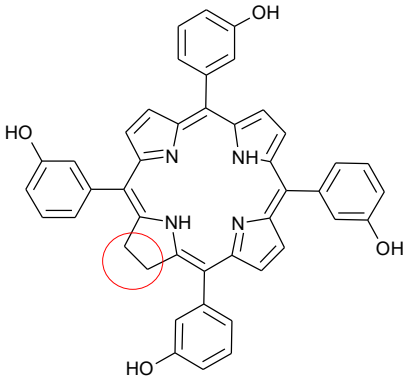

Figure 8. *Example of chlorin based PDT candidate, m-THPC (**7**).*

2.5.2 Phthalocyanines

Phthalocyanines (Pc) have analogous structure to porphyrins adding 4 benzene rings fused to pyrrole units and 4 nitrogen connecting those pyrrole rings instead of methyne bridges.

Pcs have generally high efficacy for ROS production, low dark toxicity and reach chemistry of chemical modification. Additionally, introducing coordinating diamagnetic metal atom into the inner cavity of the Pc ring has proven to increase triplet quantum yield and lifetime and produce high amount of singlet oxygen. These metals include Zn, Si, Al, Ga and In. [34]

Symmetrically substituted Pcs have been utilized for PDT. However, decreasing the symmetry of substitution increases singlet oxygen yield. [34]

One example is aluminum phthalocyanine tetrasulfonate (AlPcS4) that is sold under brand name Photosens®. It has λ_{max} value of 676 and ε_{max} of 200000 M^{-1} cm^{-1} with Φ_{Δ} being 0.38. It has been approved for use in Russia for PDT treatment of several types of cancers including skin, oral and breast cancers. However, Photosens® produces photosensitivity for skin for several weeks. [19]

(**8**)

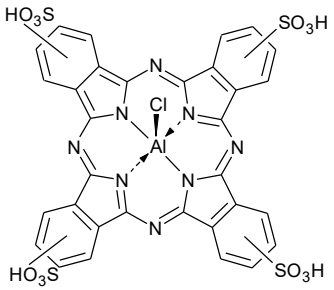

Figure 9. *Structure of AlPcS4 (**8**).*

2.5.3 Phenothiazines

Phenothiazines are a group of dyes that are based on the structure presented in Figure 10 below. They have been used as antimicrobial agents before the development of penicillin and sulfonamides. Because of their widespread use and large amount of accumulated research data they were amongst the first dyes to be utilized in PDT. Methylene blue is currently approved for photodynamic inactivation of blood plasma and blood platelets. [35]

(**9**)

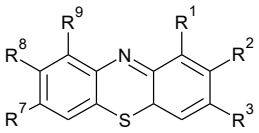

Figure 10. *General structure of phenothiazine dye (**9**).*

Methylene blue (MB) is one of the phenothiazinium family sensitizers. It has λ_{max} at 666 nm and ε_{max} 82000 M^{-1} cm^{-1}. Another example is Toluidine blue O (TBO) that has λ_{max} at 596 nm and 630 nm and $\varepsilon_{max(630\ nm)}$ 51000 M^{-1} cm^{-1}. Their advantages include low dark toxicity, cationic charge and their photophysical and -chemical properties well suited for PDT. [19]

(**10**) (**11**)

Figure 11. *Structures of Methylene blue (MB, **10**) and Toluidine blue O (TBO, **11**) respectively.*

Both molecules are well known and studied photosensitizers. They have been shown to be effective against a multitude of microorganisms. [36] These molecules have been developed further increasing their cationic nature by additional tertiary ammonium moieties. One example is methylene blue derivate in Figure 12 below. The additional cationic charge on the other side of the core group increased antimicrobial photodynamic effect when compared to MB. [37]

(**12**)

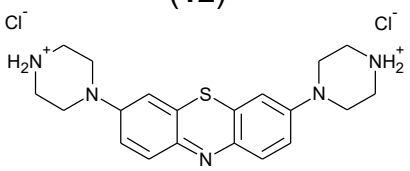

Figure 12. *Structure of 3,7-di(piperazin-4-ium-1-yl)-3,9a-dihydrophenothiazin-5-ium trichloride (**12**).*

2.5.4 Curcumin

Curcumin is one of phytochemicals found in rhizome of *Curcuma Longa* which is also known as turmeric, a common coloring and flavoring agent. This rhizome has traditionally been used as insect repellant and antimicrobial agent. Curcumin is well tolerated even in high doses of 12 g/day and it has antimicrobial, antiviral and antifungal properties. Curcumin has been extensively studied and it has been tested as antimicrobial dye for

cotton and wool. It has been used as one of active ingredients in antimicrobial skin emulsion. Curcumin has proven dark antibacterial properties and curcumin extract that were prepared from turmeric using different solvents proved to be effective in relatively low concentrations. Most efficient solvent was found to be ethanol that had minimum inhibitory concentration of 3.91-125 ppt against 24 different pathogenic bacteria that were isolated from chicken and shrimp. In addition curcumin displayed biofilm inhibiting abilities. However, poor solubility to aqueous solvents and inadequate bioavailability limit the use of curcumin as antimicrobial agent. [38]

Curcumin has λ_{max} at 420 nm and ε_{max} 55000 M^{-1} cm^{-1}. It has been proposed as a PDT substance for destroying bacteria. [19]

(**13**)

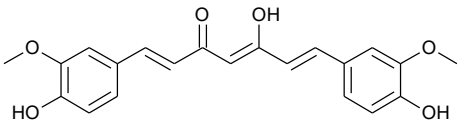

Figure 13. *Structure of Curcumin (**13**) in enol form.*

2.6 Other photosensitizers

5-Amino-4-oxopentanoic acid (5ALA) will enzymatically transform to Protoporphyrin IX (PpIX) via heme pathway when ALA prodrug is applied to skin. ALA derivatives have been proposed as drugs for cancer diagnosis in cancers affecting skin and different body cavities such as lungs, bladder and gastrointestinal tract.

5ALA is currently approved for treatment of actinic keratosis under brand name Levulan Kerasticks®. It has λ_{max} at 632 nm and ε_{max} 5000 M^{-1} cm^{-1} with Φ_{Δ} being 0.56. [19]

(**14**)

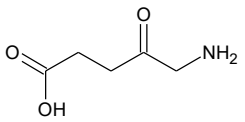

Figure 14. *Structure of 5-amino-4-oxopentanoic acid (5ALA) (**14**).*

Rose Bengal (RB) is anionic, water soluble photosensitizer with high singlet oxygen yield with exceptional effectiveness against gram (+) bacteria. [22] Polycathionic chitosan-conjugated RB was tested against gram (-) *P. aeruginosa* and it was found to be more effective than RB alone. [39]

(**15**)

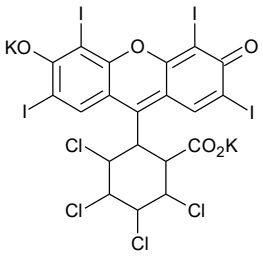

Figure 15. *Structure of Rose Bengal (**15**).*

Ruthenium (II) metal complexes, such as 1,10-phenanthroline-5,6-dione (phendione) and 2,2'-bipyridine (bpy) have presented photoactivated microbial killing effect. They have cationic structure, are water soluble and are biologically compatible. [40], [41]

2.7 Perylene derivatives as photosensitizers

Perylene diimides (PDI) derivatives have been utilized in large variety of applications due to their high thermal- and photo stability against visible light, high chemical stability and easily tuneable absorption attributes, high molar absorption coefficient and fluorescence quantum yield, nontoxicity and low cost. [10], [42] Applications for PDI derivatives include dye lasers, organic light emitting diodes, dye sensitized solar cells, organic field effect transistors and liquid crystal displays. [43]

Using different substituents in PDI, one can cover the entire visible light spectrum with their absorption spectra. [44] In addition to aforementioned applications PDI derivatives are currently used in G-quadruplex stabilization and telomerase inhibition in cancer cells. [45], [46]

Telomerase is responsible of growth of the cancer cells. It adds DNA back to telomeres thus accelerating the uncontrolled growth of tumor. G-quadruplex formation obstructs telomerase elongation *in vitro*. [47] In PDT the PS needs to be selective and accumulate to cancerous cells instead of healthy cells. This could be achieved using G-quadruplex as carrier for the PS. This makes PDIs intriguing candidate for basis of PDT agent. [48]

However, so far no perylene diimide based drugs have been proposed for PDT. Unsubstituted perylene diimides are poor photosensitizers as their intersystem crossing quantum yield is approximately $\Phi_{ISC} = 0.005$. [49] However, appropriate substituents can change this drastically. One example is perylene diimides derivate, N-(2,6-diisopropylphenyl)-N′-(3-carboxy-2-pyridyl)- 1,7-bis{4-[(4-pyrene-1-ylbutanoyl)oxy]phenoxy}perylene-3,4,9,10 -tetracarboxylic diimide (PDI-Pyr, **16**) which has shown singlet oxygen quantum yield of $\Phi_{\Delta} = 0.93$. [47]

In addition PDI-Pyr and N-(2,6- diisopropylphenyl)-N′-(3-carboxy-2-pyridyl)-1,7-bis{4-[(4-in- dole-3-ylbutanoyl)oxy]phenoxy}perylene-3,4,9,10- tetracarboxylic diimide (PDI-

In, **17**) both showed DNA binding affinity from their side chains. This was due to their nitrogen and oxygen groups in their cationic forms. In addition the G-quadruplex binding could be applied to deliver the PDI-Pyr to cancer cells. [47]

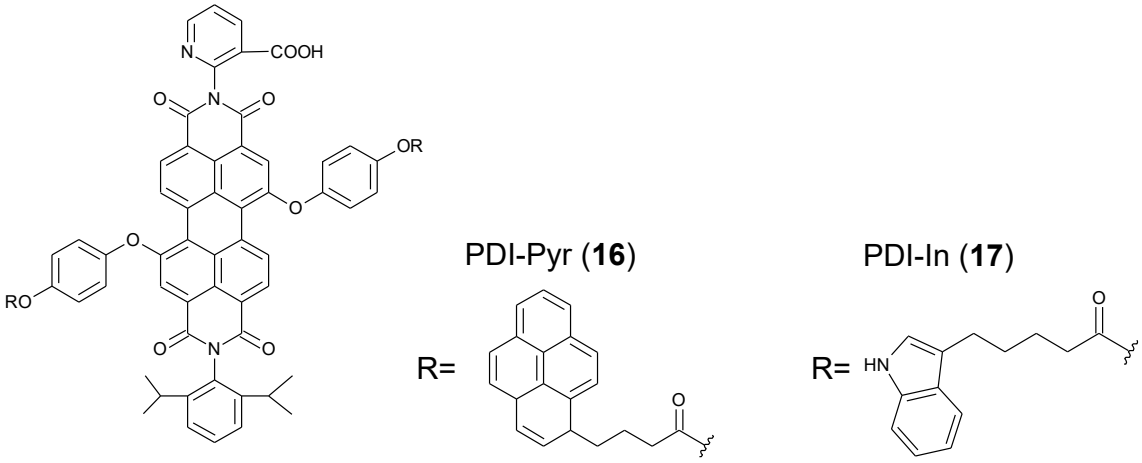

Figure 16. *Structures of PDI-Pyr and PDI-In. Both of these unsymmetrical PDIs present promising singlet oxygen quantum yields.*

Possibility to adjust absorption, high singlet oxygen quantum yield and the ability to target cancer cells make PDIs an interesting and promising candidate for PDT. Similar attributes are needed in PACT applications.

3. RESULTS AND DISCUSSION

Some perylene diimide derivatives show promising features for ROS generators and a study conducted by Dinçalp et al. reported these examples. [47] More study is still required in this field as only a few such examples exist.

Purpose of this thesis was to synthesize new molecules that could be later tested for their ability to generate ROS. Synthetic plan consisted of three lines that all shared the same first two synthetic steps. The schemes are presented in APPENDIX A.

Perylene-3,4,9,10-tetracarboxylic dianhydride (PTCDA) consists of 2 carboxylic anhydride groups that are at peri-positions of perylene molecule. These parts are marked with blue and red color circles in Figure 17 below.

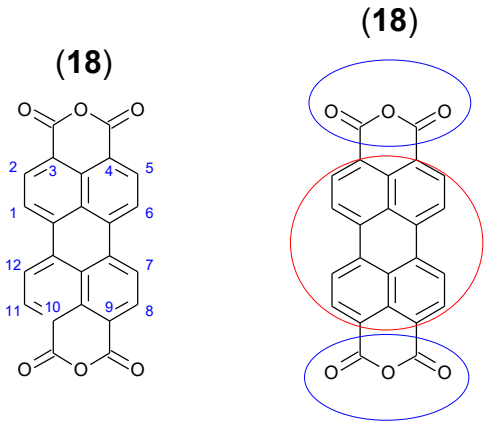

Figure 17. *Structure of PTCDA (**18**) molecule. On the left side its carbons are numbered and on the right side its different functional parts are emphasized with colored circles.*

PTCDA is insoluble in organic solvents. This is due to the extensive face-to-face π-π stacking of these molecules. [50] However, it can be dissolved in concentrated sulfuric acid. This is true for nearly all perylene pigments and it happens via protonation. [51]

The aromatic carbons in the perylene core form a characteristic cavity, so called "bay area". It corresponds to the positions 1,6,7,12 of PTCDA. Later "1,6- and 1,7- isomers" will refer to substitution in these bay-area positions.

3.1 Original plans for synthesis

Synthetic scheme consisted of three plans. All of the plans started with same two steps. These steps are given in the Figure 18 below.

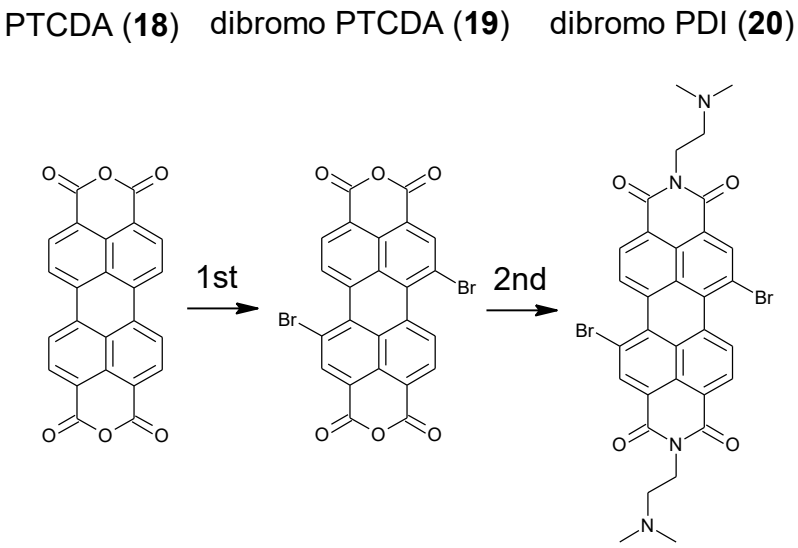

Figure 18. *The two first synthetic steps. The dibromo PDI (**20**) was common starting material for all consecutive synthetic schemes.*

First target molecule was quaternary salt of 1-pyrrolidine,7-carbazole PDI. First two synthetic steps were conducted without any difficulties. However, the third step proved very problematic. Last three steps of the first plan can observed in the Figure 19 below. These attempts are disclosed in greater detail in chapter 3.3

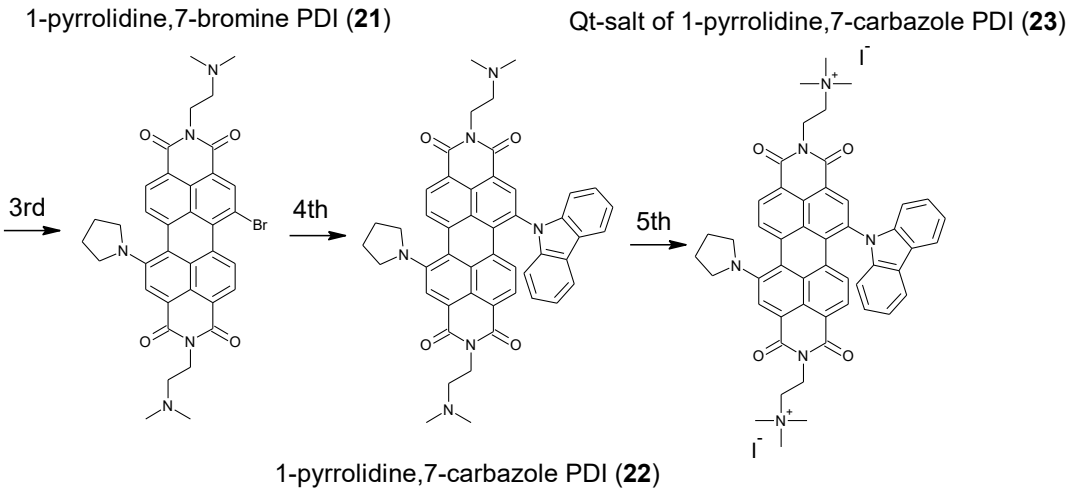

Figure 19. *The last three steps of the first synthetic plan.*

Second target molecule was quaternary salt of disulfonyl-4-pyridine PDI. This synthesis was performed up to the second to last step without any insurmountable difficulties. However, after the sulfonating step the product was found to be water soluble. This was surprising and because of limited time this could not be purified. Therefore thiol-4-pyridine PDI was quaternized to produce cationic dye.

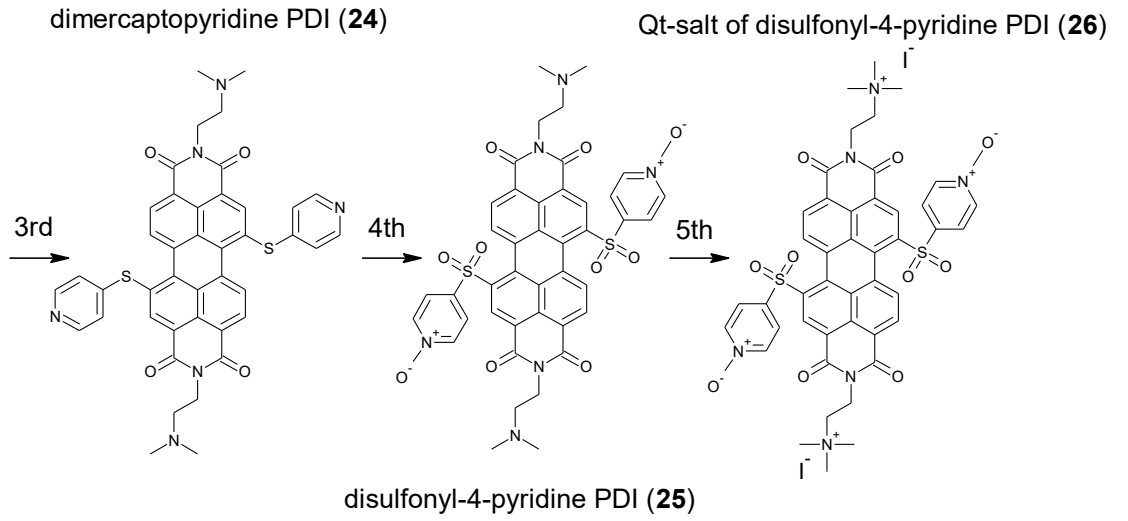

Figure 20. *Last three synthetic steps of the second synthetic plan.*

Third target molecule was quaternary salt of PDI with 1,7-bis(4-hydroxyphenyl 3-(pyren-1-yl)propanoate) (HPP-PDI) substituents. Here again the third synthetic step, hydroquinone substitution, proved difficult. This was due to possible polymerization of the PDI units as the hydroquinone could react with both ends. Product could not be purified with CC as it would not pass the column. To circumvent this issue, hydroquinone was attempted to mono-protect in order for it to react with only one end. This proved to be too challenging. Therefore this plan was abandoned. Third plan can be observed in below Figures 21 and 22.

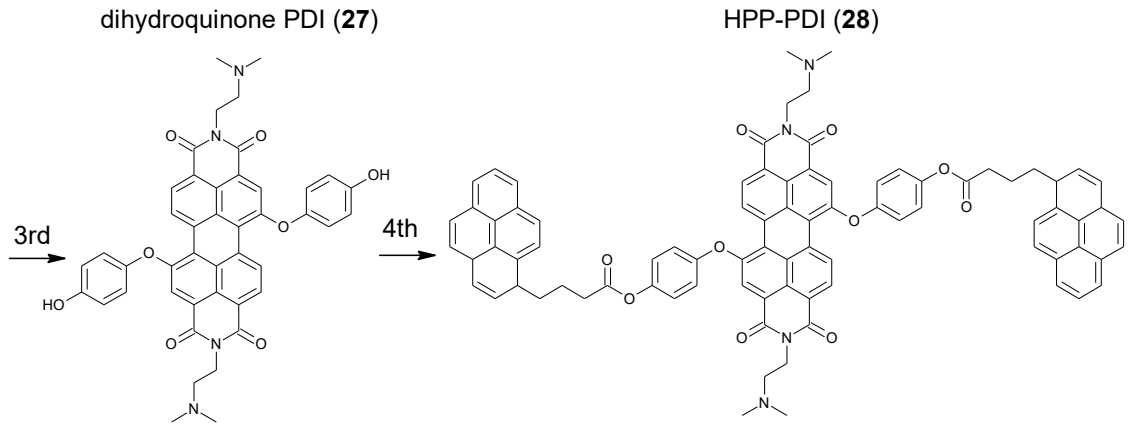

Figure 21. *The 3rd and 4th step of third synthetic plan.*

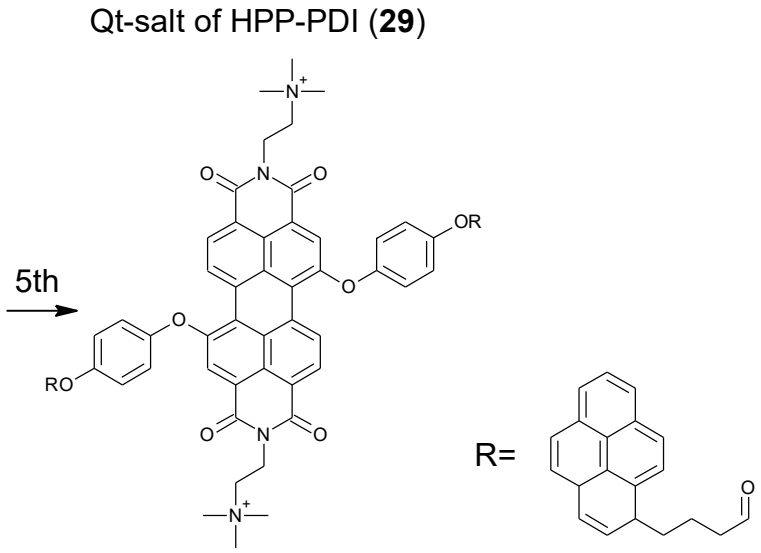

Figure 22. *The 5th step of third synthetic plan.*

3.2 Accomplished synthesis

This chapter describes in detail the synthetic scheme to produce Qt-salt of dimercapto-pyridine PDI.

3.2.1 Synthesis of dibromo PTCDA

Reaction scheme started with introduction of bromine atoms to bay area of PTCDA to produce compound **19**. Target was 1,7-dibromo perylene-3,4,9,10-tetracarboxylic di-anhydride (dibromo PTCDA). Bromine is needed in order to introduce functional groups to bay area positions later. This also increased the solubility of compound to organic solvents by bending the core structure and adding large substitute atoms to bay area positions. This decreased the face-to-face π-π stacking of these molecules. [52] This made PTCDAs soluble to chloroform. [50]

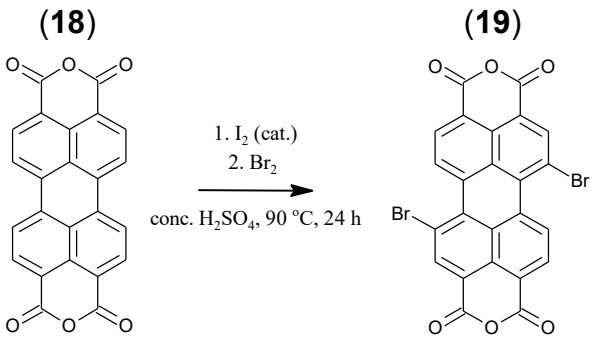

Figure 23. *Synthesis of dibromo PTCDA (**19**) using PTCDA (**18**) as starting material.*

In the first step starting material was dissolved in concentrated H_2SO_4. This was done by stirring the solution for 24 hours (h) in room temperature (RT). The red solid seemed to have dissolved completely in the acid. In the next step iodine was added in to solution of PTCDA. Iodine was added before bromine in order for it to react with PTCDA. Iodine acted as catalyst for subsequent bromination. Bromine evaporated strongly during addition giving out brown toxic and caustic fumes. Because of this strong activity, bromine was added all at once. This addition were done under fume hood. After adding iodine and bromine heating was started. Reaction was kept at 90 °C for 24 h.

After heating was removed and vial had cooled to RT, the cap was opened. There were visible brown colored fumes released from the vial. Vial was placed tilted near the exhaust of the fume hood and left there for one hour.

A total of 2.0 ml of water was added to reaction vial to precipitate the product out. Some product however remained in solution. This was very exothermic reaction and therefore vial was placed in to water bath to cool it down. Added a bit more water and then transferred product in to №4 filter using water. (See Table 3 for pore size)

A total of 12 ml of 80 % H_2SO_4 was prepared using concentrated H_2SO_4 and water. This was performed using 10 ml of H_2SO_4 to which 2 ml water was added dropwise. This prepared 80 % H_2SO_4 solution was used to wash the product (**19**). Filtrate had strong red coloring and it was once more filtered.

Second filtering is more promising as filtrate is now clear. Water is used to wash product and precipitate is agitated with spatula during washing. Washing is continued until pH of waste water is around the same as the used washing water.

Product was dried on filter using suction and after that it was placed in to vacuum desiccator. At this point product was not purified as the isolation of 1,7- and 1,6- isomers is not possible using column chromatography because of poor solubility. [53]

3.2.2 Synthesis of dibromo PDI

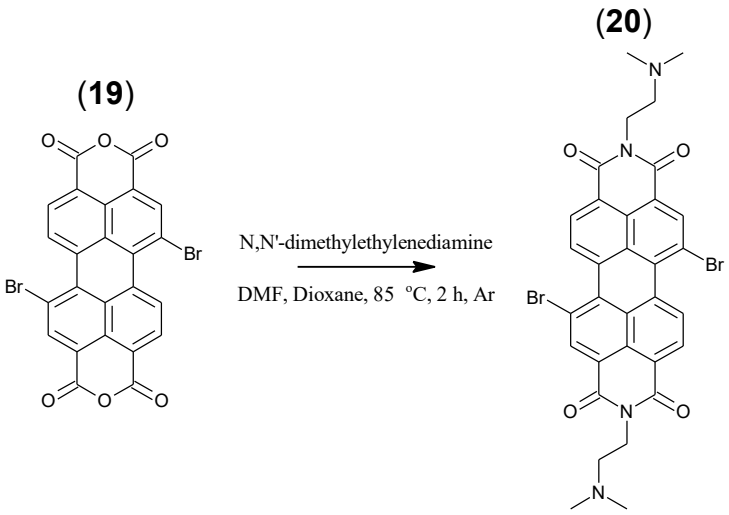

Figure 24. *Synthesis of dibromo PDI (**20**) from dibrominated PTCDA (**19**).*

Imidation of dibromo PTCDA was done using dry dibromo PTCDA as starting material. In this synthesis the anhydride cycles of the molecule react with the amine creating dibromo-perylene diimide (dibormo PDI). This particular amine was selected because it can be quaternized later, making the molecule water soluble.

Synthesis was performed under argon gas (Ar). Starting material was added in to vial with a stirring bead. Vial was closed with a cap that had 3 small holes on top of it. Gentle Ar-flow was applied through the cap with 2 needles connected to silicon hose. Flow of Ar was controlled with bubbling it through oil. Solvents were added with syringes and needles through the 3rd hole in the cap. After this stirring was started. Last the N,N-dimethylethane-1,2-diamine (DMEN) was added with syringe and needle through the 3rd hole. After this heating was started and when temperature had reached around 70 °C the Ar flow was stopped and cap sealed with parafilm. Heating was continued until reaction temperature was reached. Reaction was kept at 85 °C for 2 hours and after that heating was removed. During this time the color changed from bright red to dark red/violet. The color can be observed in Figure 25 below.

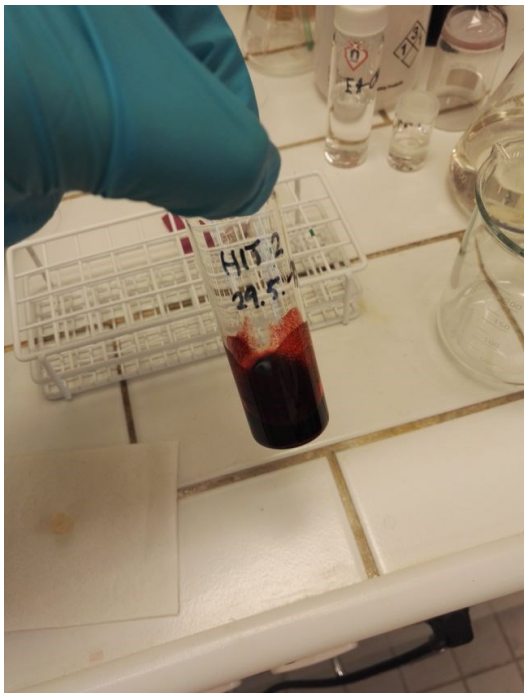

Figure 25. *Vial containing component* ***19*** *after cooling back to RT.*

After vial had returned to RT water was added to precipitate the product and stop the reaction. The precipitate was filtered off on №4 filter and washed with water several times with applied suction. Filtering proved extremely difficult and excess solvents were removed with rotary evaporator.

Precipitate was dried in vacuum desiccator and dissolved in minimum amount of chloroform. Product was purified using column chromatography (CC). The product had strong red color wich can be seen in the Figure 26 below. Column was prepared using 50 ml of silica 100. Column was packed using pure $CHCl_3$ and silica. At the beginning pure $CHCl_3$ was used to drive the product. Gradually the polarity of the eluent was increased until the final composition of eluent was $CHCl_3$:EtOH:Et_3N (93:6.5:0.5). One major fraction was collected and it was found to contain mixture of 1,7- and 1,6- isomers of dibromo PDI **20**, as proved by high-resolution mass spectrometer (HRMS) and nuclear magnetic resonance (NMR). However, this isomeric mixture was deemed pure enough for subsequent synthetic steps and possibility of isomeric purification with CC was higher with larger bay-area substitutes. [54]

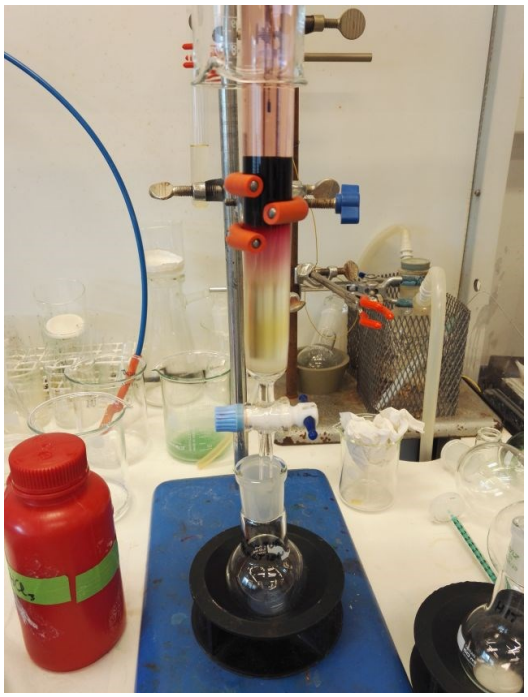

Figure 26. *Column chromatograph setup used in purification of dibromo PDI* ***(20)****.*

HRMS results can be observed in APPENDIX B. Below in Figure 27 is the NMR spectrum of dibromo PDI.

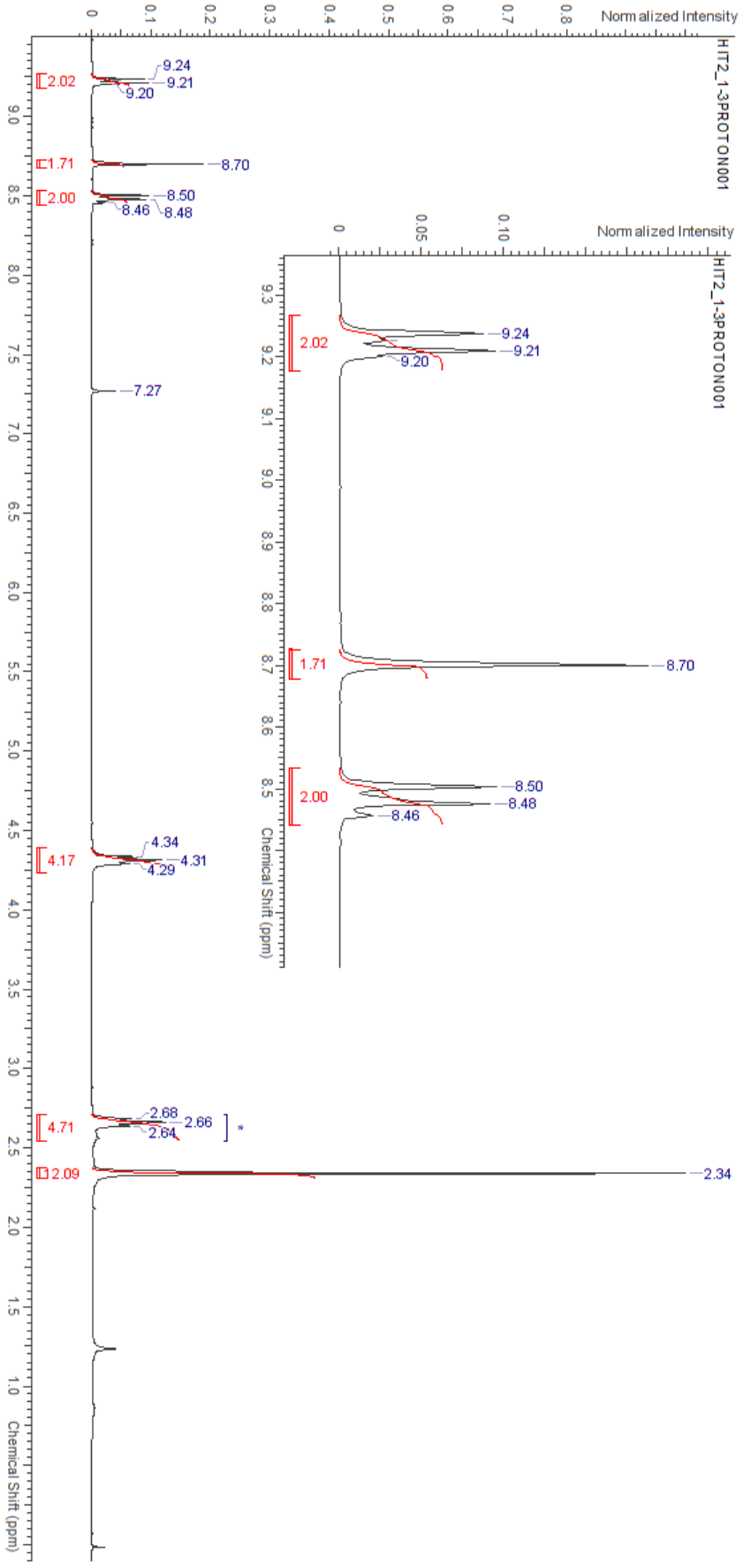

Figure 27. *^{1}H NMR spectrum of dibromo PDI* ***(20)*** *in $CDCl_3$.*

Aromatic region in the ^{1}H NMR spectrum of dibromo PDI shows signals that are multiplets instead of clear doublets. This can be observed for signals at chemical shift 9.24 ppm (J=8.19 Hz) and 8.50 ppm (J=8.19 Hz). Singlet at 8.70 ppm which corresponds to the protons connected to carbons 2 and 8 is not repeated in any other location. It might have different value for 1,6-isomer, but whether this is the case remains unknown. The triplet located at 4.31 ppm corresponds to CH_2 that are next to the imide nitrogen and triplet at 2.66 ppm corresponds to the other CH_2 group in the imide tails. Singlet at 2.34 corresponds to the 12 protons that are in the 4 methyl groups which are connected to the amines.

MS (ESI-TOF) [M+H] signals: found 691.0353, calculated 691.0381, lock mass 556.2771, Accuracy 3.0 ppm. These results, in conjunction with the above NMR test results, confirm the presumed structure of target molecule.

3.2.3 Synthesis of dimercaptopyridine PDI

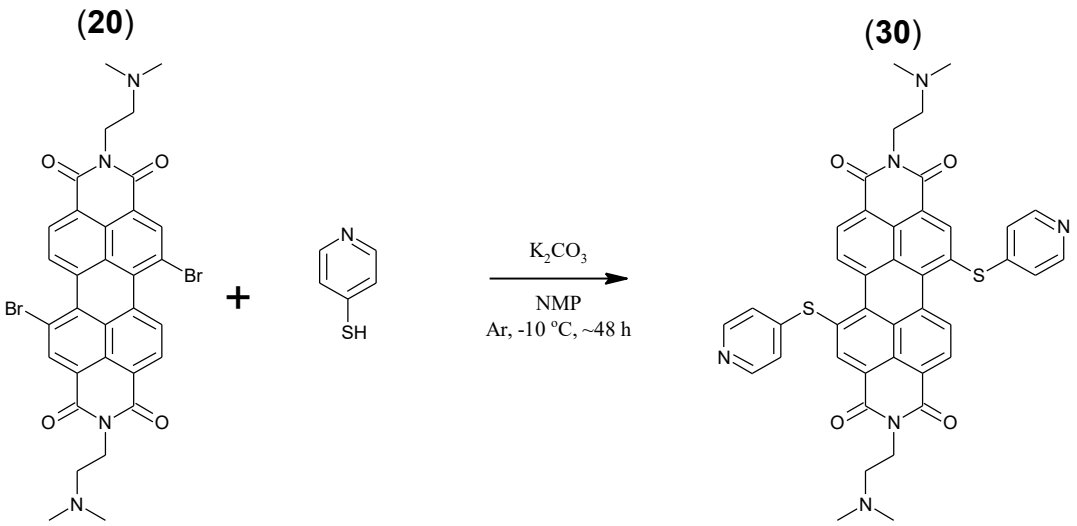

Figure 28. *Synthesis of dimercaptopyridine PDI (**30**).*

Dibromo PDI was used as starting material for synthesis of dimercaptopyridine PDI. Dry potassium carbonate acted as base it the reaction. Reaction was performed at low temperature following procedure from literature. [44] This was achieved using insulated ice bath with ice/NaCl mixture that is shown in the Figure 29 below.

Figure 29. *The setup for chilled reaction.*

Ice and salt were mixed in a plastic bowl before adding this mixture to insulated vessel. This guaranteed sufficient mixing of salt and ice and led to below freezing temperature of this cooling bath. Reaction time was around 3 hours and despite of all the insulation the ice slowly melted. This was countered by removing water and adding ice/NaCl mixture to the ice bath approximately twice per hour. TLC was preformed to in order to define the progress of the reaction and reaction deemed complete after 3 hours. Water was added to vial to precipitate the product. Mixture was filtered on №4 filter and it was left there to pass though the filter overnight. Filtrate was strongly colored and NaCl was added to filtrate to precipitate the product out. This helped and the next filtering was successful.

Column was prepared using 30 ml of silica 100 and using $CHCl_3$:EtOH:Et_3N (93:6.5:0.5) as eluent. However, this did not produce desired separation as can be seen in Figure 30 below. In Figure 30 several different components can be observed and they are numbered in the upper plate. Search for suitable stationary phase/eluent-combination produced alumina/ $CHCl_3$:EtOH (100:1) as best option.

Figure 30. *TLC plates used to determine suitable stationary phase/eluent combination. TLC was developed using starting material, co-spot and product, which had been CC purified before.*

Because the amount of product was small enough, the purification was done using TLC on alumina plates. This method produced relatively good separation of components.

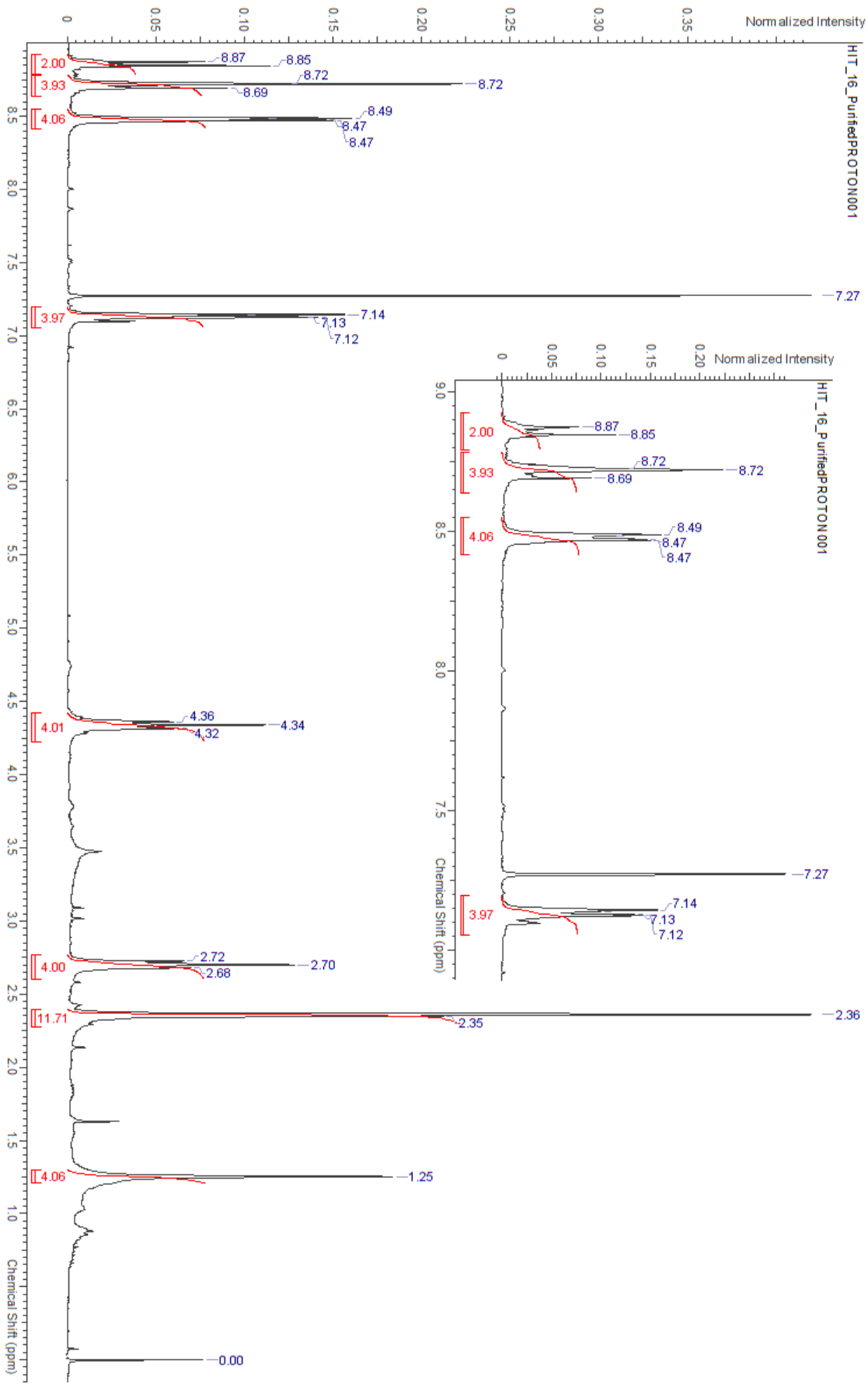

Figure 31. *^{1}H NMR spectrum of dimercaptopyridine PDI (**30**) in $CDCl_3$.*

NMR experiments were conducted using $CDCl_3$ as solvent. This solvent contains trimethylsilane (TMS) as internal standard. The ^1H NMR spectrum was corrected using values 7.27 ppm for $CDCl_3$ and 0.00 ppm for TMS. From the spectrum it is evident that this substance is not pure 1,7-isomer.

Signals with chemical shift 2.33-2.39 ppm correspond to methyl groups connected to amine tails at the peri-positions. This signal was expected to be singlet, but due to shimming issues signal is not completely clear. Additionally some aliphatic impurities are present and these produce signal with chemical shift of 1.25 ppm. Two triplets at 2.70 ppm and 4.34 ppm correspond to the CH_2 groups of these peri-position imide tails. The shifts are close to what was observed in starting material.

Aromatic part is problematic as it would be expected that the protons connected to the perylene core would have different chemical shifts from each other. If this were true, it would create: 2 doublet signals with differing chemical shifts and integral values of 4, 2 singlet signals with integral value of 2 and 2 doublet signals with integral value of 2. These 2 doublet signals would correspond to the CH groups located in pyridine moieties, 2 singlet signals would correspond to the CH groups located in perylene core numbered 2 and 8 and 2 doublet signals would correspond to the CH groups located in perylene core numbered 5, 6, 11 and 12.

Aromatic part is unclear because of presence of both 1,6- and 1,7-isomers and due to shimming issues.

3.2.4 Synthesis of quaternary (Qt-) salt of dimercaptopyridine PDI

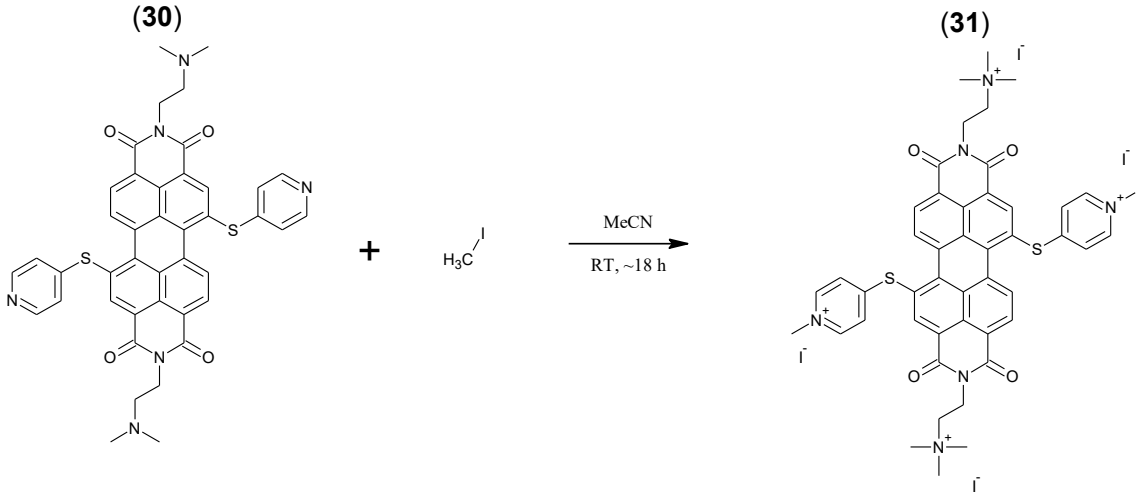

Figure 32. *Quaternarization of dimercaptopyridine PDI (**31**).*

Quaternarization was conducted using large excess (~600 eq) of methyl iodide (MeI). The progress of this reaction was followed by TLC but this proved difficult. There was no way to tell if all quaternizable nitrogen atoms had reacted. Reaction was stopped after 18 hours and product was precipitated using diethyl ether. Ether was used to wash product several times on watch glass to remove any remaining MeI and MeCN.

After drying the product, MS was used to determine the mass to charge ratio of product. The mass to charge ratio from MS (ESI-TOF) measurements proved that some molecules had not completely quaternized. Therefore quaternarization was performed again to this product to ensure full quaternarization.

This time the reaction was conducted using N,N-Dimethylformamide (DMF) as solvent. Again large excess (~300 eq) of MeI was used. Reaction was conducted in RT and it was stirred for around 16 hours. After this the same ether precipitation and washing was conducted to remove unreacted materials and excess solvents. HRMS was used to determine that quaternarization had completed.

3.2.5 Verification of the structure of the target molecule

This molecule was verified using MS (ESI-TOF) and NMR. Mass spectrum was interpreted by first checking the number of charges for every signal obtained. This can be calculated from the distance between peaks in isotopic patterns. ESI-TOS gives mass to charge ratio (z/m) signals from substance. Therefore substance, like our Qt-salt of dimercaptopyridine PDI, that has 4 charges will have 0.25 Dalton (Da) difference between signal maximums. However it became evident that this salt was not completely ionized and instead charge numbers 2 and 3 were observed with masses corresponding additional iodine atoms.

UV-Vis spectrum showed absorption maximum λ_{max} at 530 nm with molar attenuation coefficient ε of 24344 ($M^{-1}cm^{-1}$). Measurements were conducted in water.

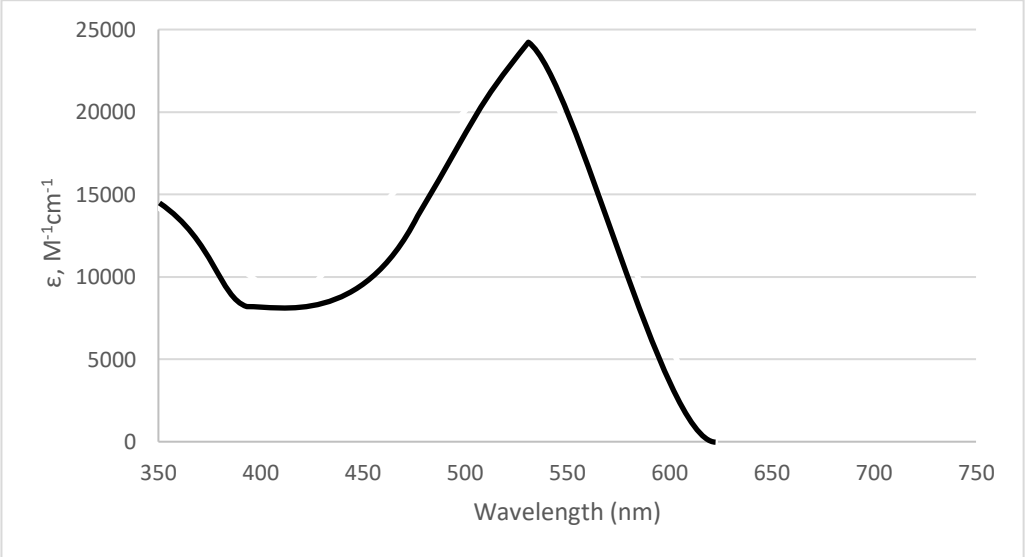

NMR spectrum was adjusted with D_2O solvent peak at 4.75. Signal observed at 2.68 ppm was believed to correspond to trace amounts of DMF. [55]

Spectra that were measured: ^{1}H, ^{13}C, COSY (COrrelation SpetcroscopY), gHSQC (gradient Heteronuclear Single Quantum Correlation) and gHMBC (gradient Heteronuclear, Multiple Quantum Correlation).

From these signals gHSQC and gHMBC had poor signal to noise ratio in aromatic region. Therefore some proton and carbon signals were not able to be paired definitively.

COSY gives signals of coupled protons. It shows proton signals that are at neighboring carbons away from each other and thus gives information on structure on the molecule. This is called scalar coupling by the way, *J*-coupling

HSQC gives signal that correlate chemical shifts of proton connected to other nucleus via J-coupling. From gHSQC spectrum it is possible to determine type of carbon-proton system, as positive signals correspond to CH and CH_3 systems and negative signals correspond to CH_2 and CH_4 systems. These values are presented with (+) and (-) respectively.

HMBC assigns ^{1}H and ^{13}C signals based on long-range *J*-coupling. From this spectrum it is possible to determine which carbons are close to, but not connected to, which protons. Signal is based on system of $^{n}J_{CH}$ where N>1.

(31)

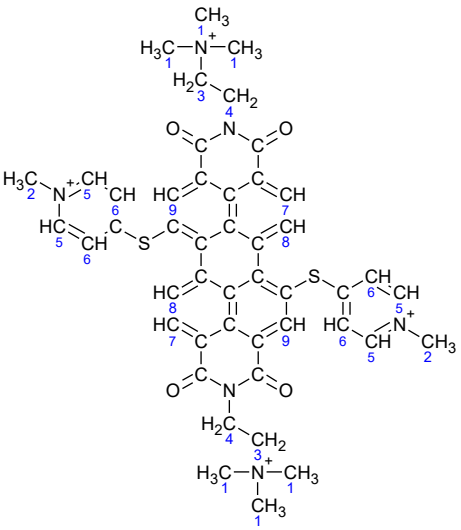

Figure 33. *Molecule of Qt-salt of mercaptopyridine PDI (**31**) where all carbon atoms corresponding to 1H NMR signals are numbered. Numbering is given to aid interpretation.*

From proton signal (^{1}H) integral values it was possible to determine that structure corresponds to molecule with this amount of protons. Signal shows smaller doublets around aromatic part of proton signal. This was interpreted that sample contains both 1,6- and 1,7-isomers.

NMR ^{1}H signal can be observed in Figure 34 below. This spectrum is interpreted using 2D NMR spectra from Figure 35, Figure 36 and Figure 37 in Table 1 below. Here Carbon-proton pair number refers to numbered carbons in Figure 33. Chemical shift corresponds to signals of 1H spectrum in Figure 34. Rounded integral number corresponds to number of protons for observed chemical shift, signal type is the signal multiplicity and J-values are the spin-spin coupling values for multiplet signals, and they are from the same aforementioned spectrum.

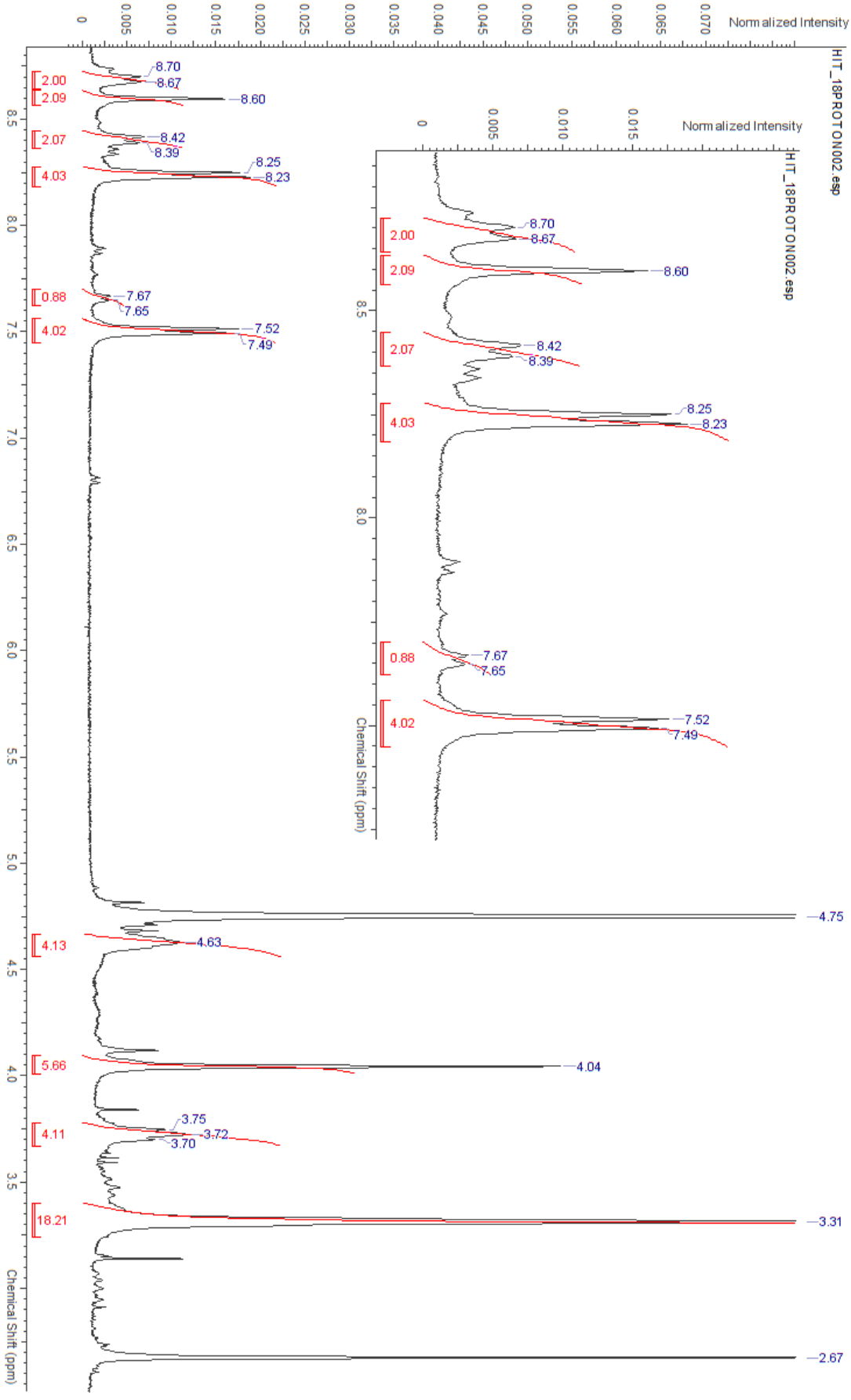

Figure 34. *^{1}H NMR spectrum of Qt-Salt of dimercaptopyridine PDI (**31**) in D_2O.*

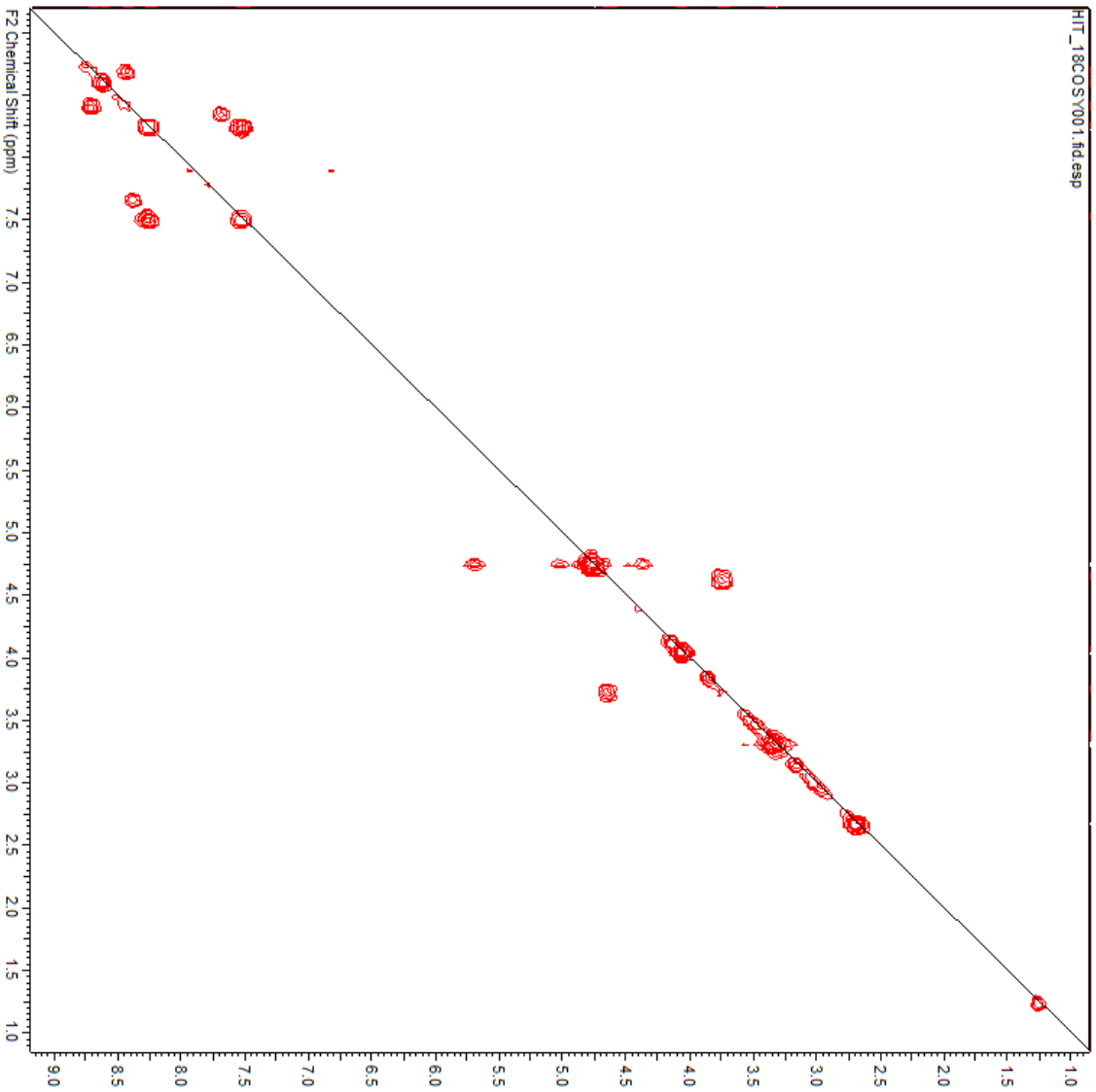

Figure 35. *COSY NMR spectrum of Qt-Salt of dimercaptopyridine PDI* ***(31)*** *in D2O.*

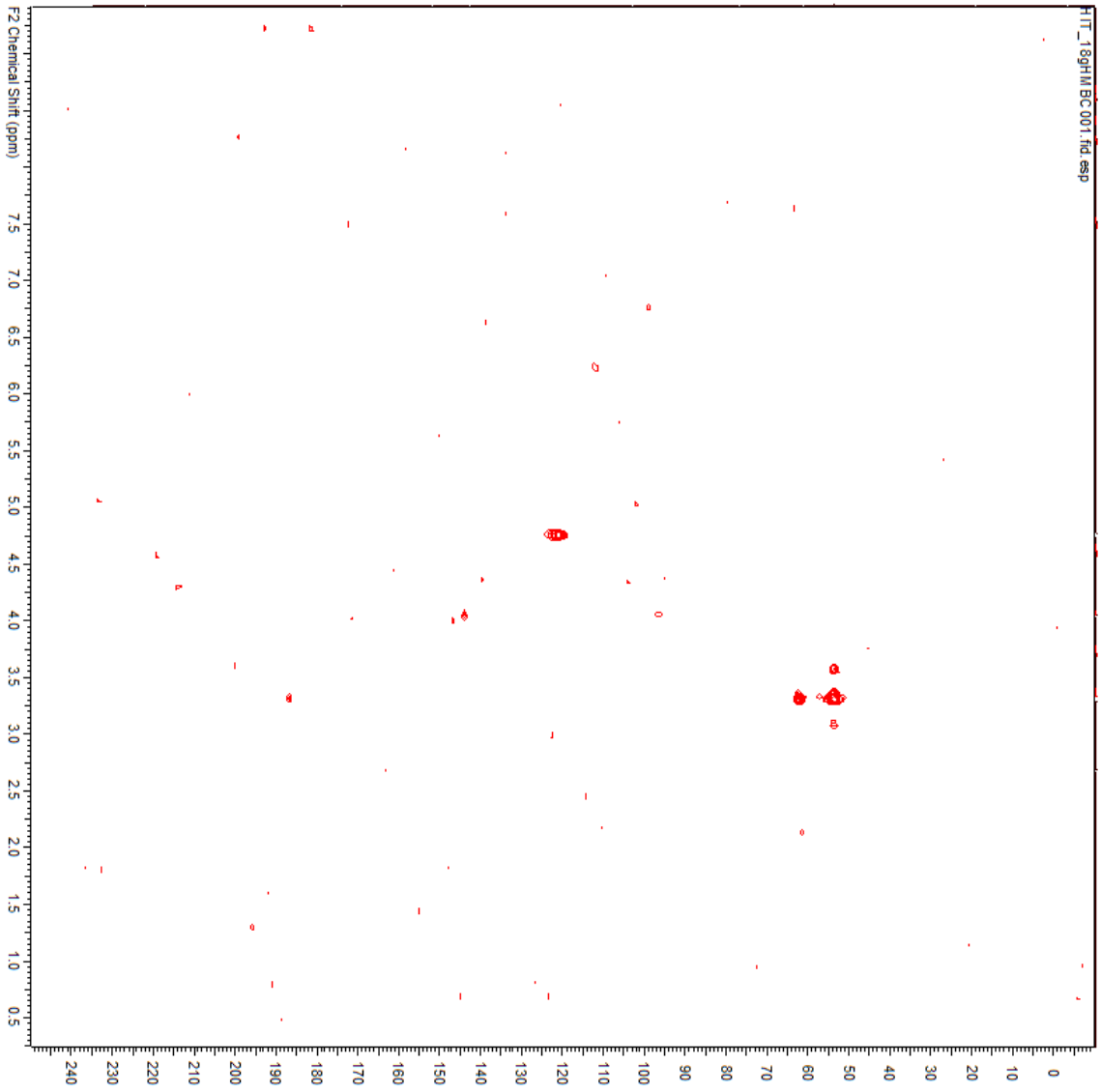

Figure 36. *HMBC NMR spectrum of Qt-Salt of dimercaptopyridine PDI (**31**) in D2O.*

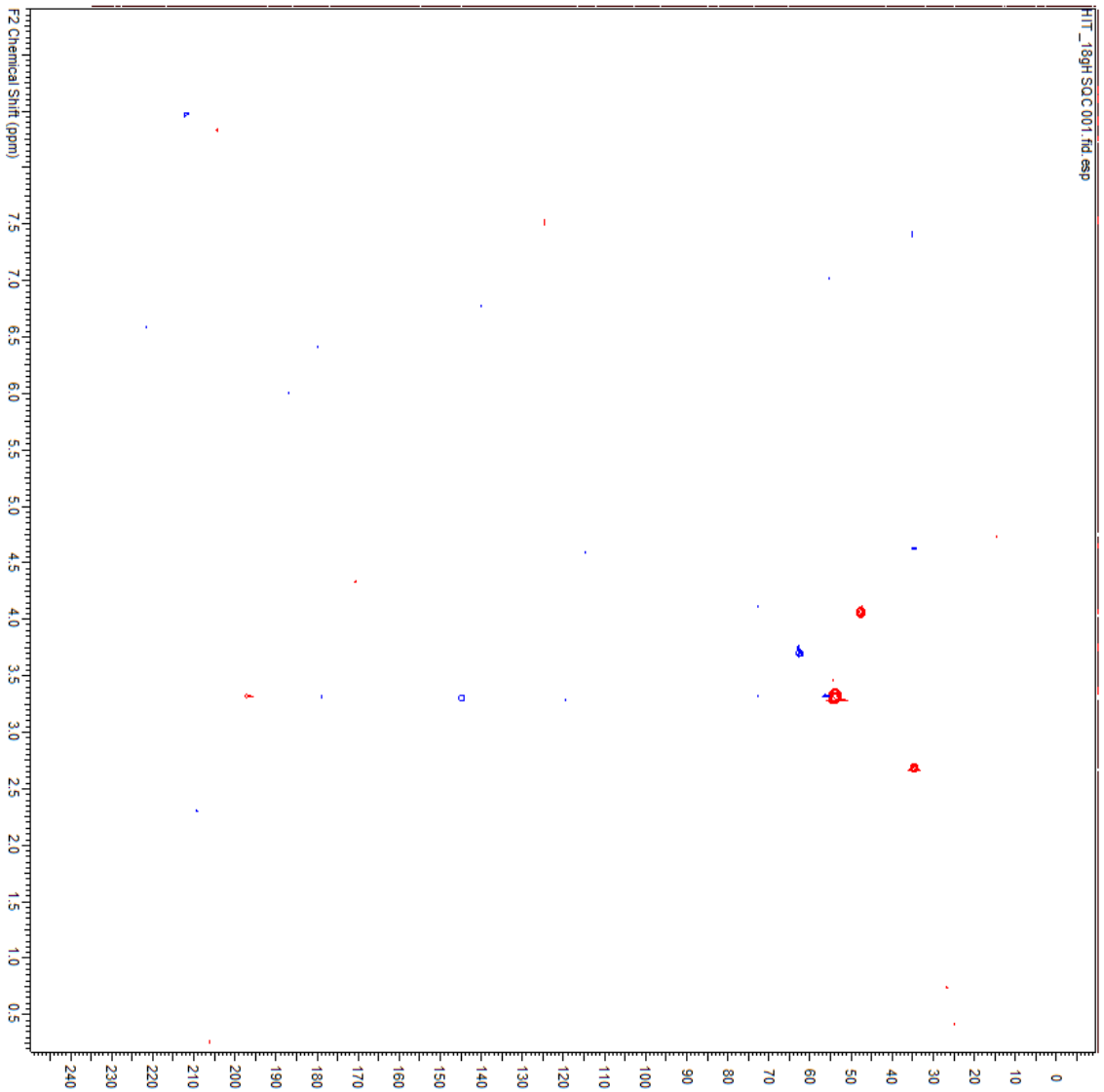

Figure 37. *HSQC NMR spectrum of Qt-Salt of dimercaptopyridine PDI (**31**) in D2O.*

Table 1. *1H NMR-spectrum interpretation of Qt-salt of dimercaptopyridine PDI (**31**).*

Carbon-proton pair number	Chemical shift ^{1}H (ppm)	Normalized integral (number of H)	Signal type	J-value (Hz)	Coupled to (from COSY)
1	3.31	18	singlet	-	-
2	4.04	6	singlet	-	-
3	3.72	4	triplet	7.02	4
4	4.63	4	triplet	5.27	3
5	8.25	4	doublet	7.02	6
6	7.52	4	doublet	6.44	5
7 ?	8.42	2	doublet	8.19	8
8 ?	8.70	2	doublet	8.19	7
9	8.60	2	singlet	-	-

COSY spectrum gave further confirmation on the selected numbering. After COSY only uncertainty left was the order of carbon-proton pairs 7 and 8. Unfortunately the resolution of gHSQC and gHMBC spectra did not give definite answer to this question.

Carbon-Proton pairs of signals that were determined from gHSQC and gHMBC are presented in Table 2 below.

Table 2. *Signal pairs from gHSQC and gHMBC NMR experiments. Paired proton and carbon shifts are given and sign is given for gHSQC signals.*

Signal pairs			
HSQC			
proton	carbon	pos/neg	
2.67	34.32	+	
3.31	53.42	+	
3.71	62.07	-	
4.04	47.16	+	
4.61	33.24	-	
7.5	124.17	+	
8.3	203.77	+	uncertain

HMBC		
proton	carbon	
3.31	53.4	
3.31	62.1	
4.04	144	
3.31	185	uncertain

To get more information on expected ^{1}H NMR spectra the molecule was modeled using computational method. Software used was PerkinElmer ChemBioDraw, Level: Ultra, Version: 13.0.0.3015.

Molecule was modeled using built in feature that calculates ^{1}H NMR spectra in $CDCl_3$ and in DMSO-d_6. However, the NMR spectroscopy was done using D_2O as solvent and therefore these models were only be used as general guides. This modeling gave identical results for both solvents except for the signal coming from CH group number 8. This signal was shifted from 8.06 to 8.12 when modeling with $CDCl_3$ and DMSO-d_6 respectively. This modeling provided reasonable guidelines for what kind of shifts and signals to expect.

Computational model would suggest, that proton signal in CH number 8 is more shifted than in CH number 7.

3.3 Results from first synthetic plan

Several attempts were made on first synthetic plan. However, the mono-pyrrolidine substitution of PDI was not achieved and problems aroused in subsequent purification of the compound. Several attempts were made but they proved unsuccessful. Second step would have been the addition of 9H-carbazole to the other side of perylene molecule. To circumvent this issue, mono 9H-carbazole substitution was tried before pyrrolidine substitution, but even this approach did not produce monosubstituted molecule with any decent yield.

First reactions were performed using pyrrolidine as substituent.

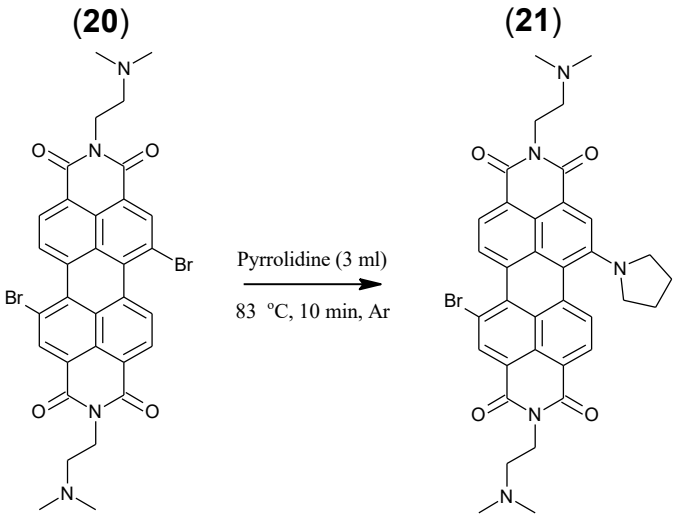

Figure 38. *First attempt to follow the first synthesis plan. Target molecule was 1-Bromo,7-pyrrolidine PDI.*

Product was purified using CC. Stationary phase was silica 60 and eluent $CHCl_3$:EtOH 9:1. However, this combination proved to be cumbersome and following purification attempts were performed using silica 100 and $CHCl_3$:EtOH:Et_3N 93:6,5:0,5. This modification improved the moving and separation of different components. After purification the collected components were tested using MS (ESI-TOF). Major product was discovered to contain mainly dipyrrolidine PDI. Results can be observed in below Figure 39.

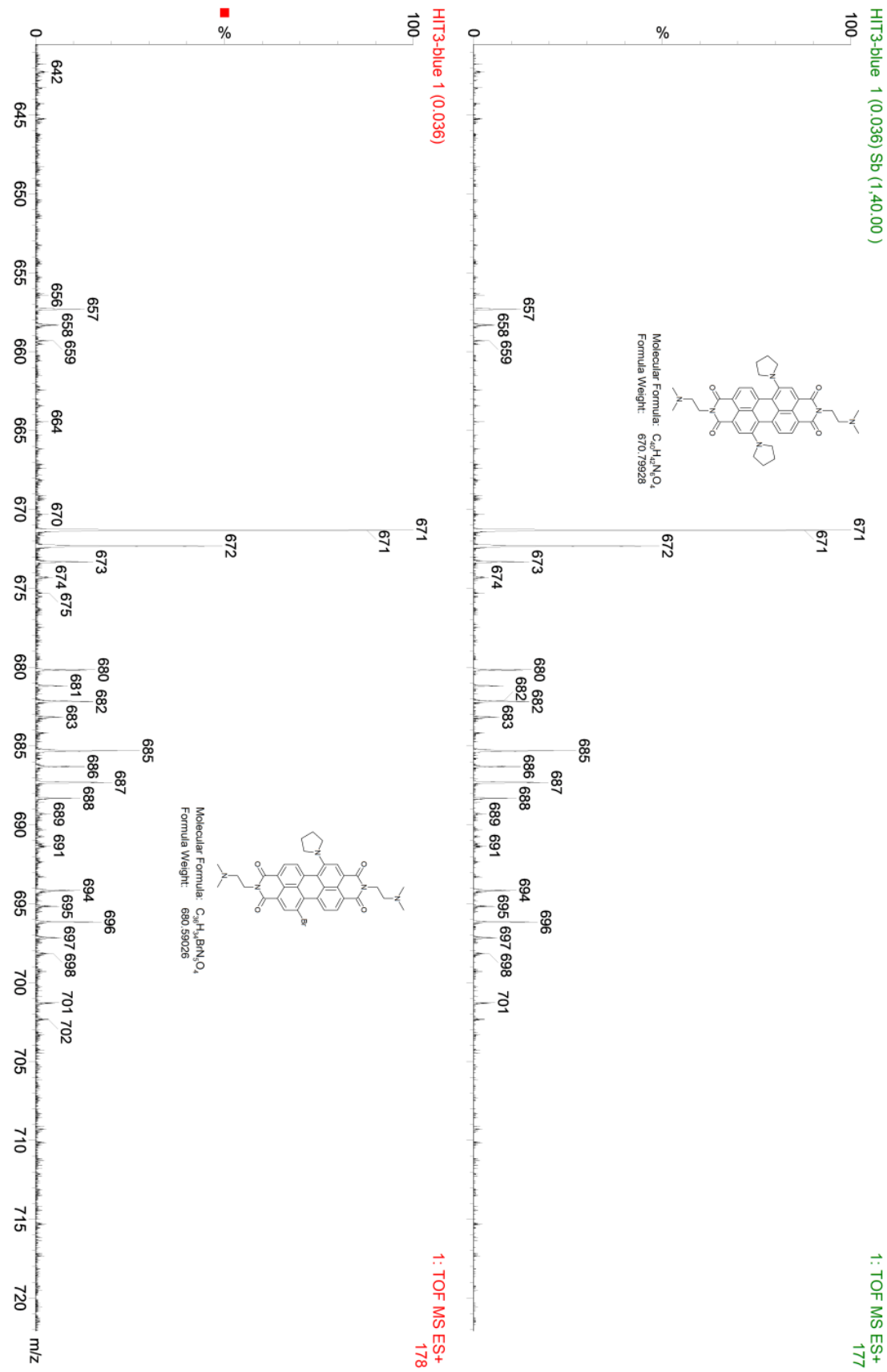

Figure 39. *MS (ESI-TOF) Results after first pyrrolidine reaction. Target molecule is observed at around 680 m/z.*

This pyrrolidine substitution reaction was repeated using temperature of 0°C and reaction time of around 4 hours. While the product can be observed in MS (ESI-TOF), the NMR results were inconclusive. This was possibly due to extremely low amount of product.

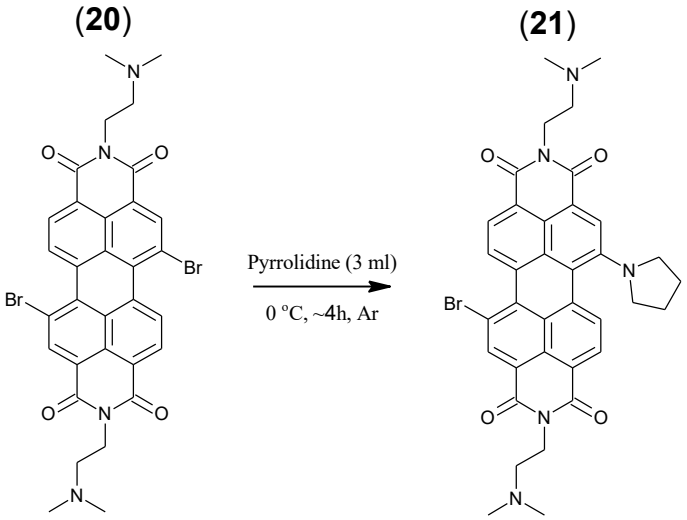

Figure 40. *Second attempt on pyrrolidine monosubstitution.*

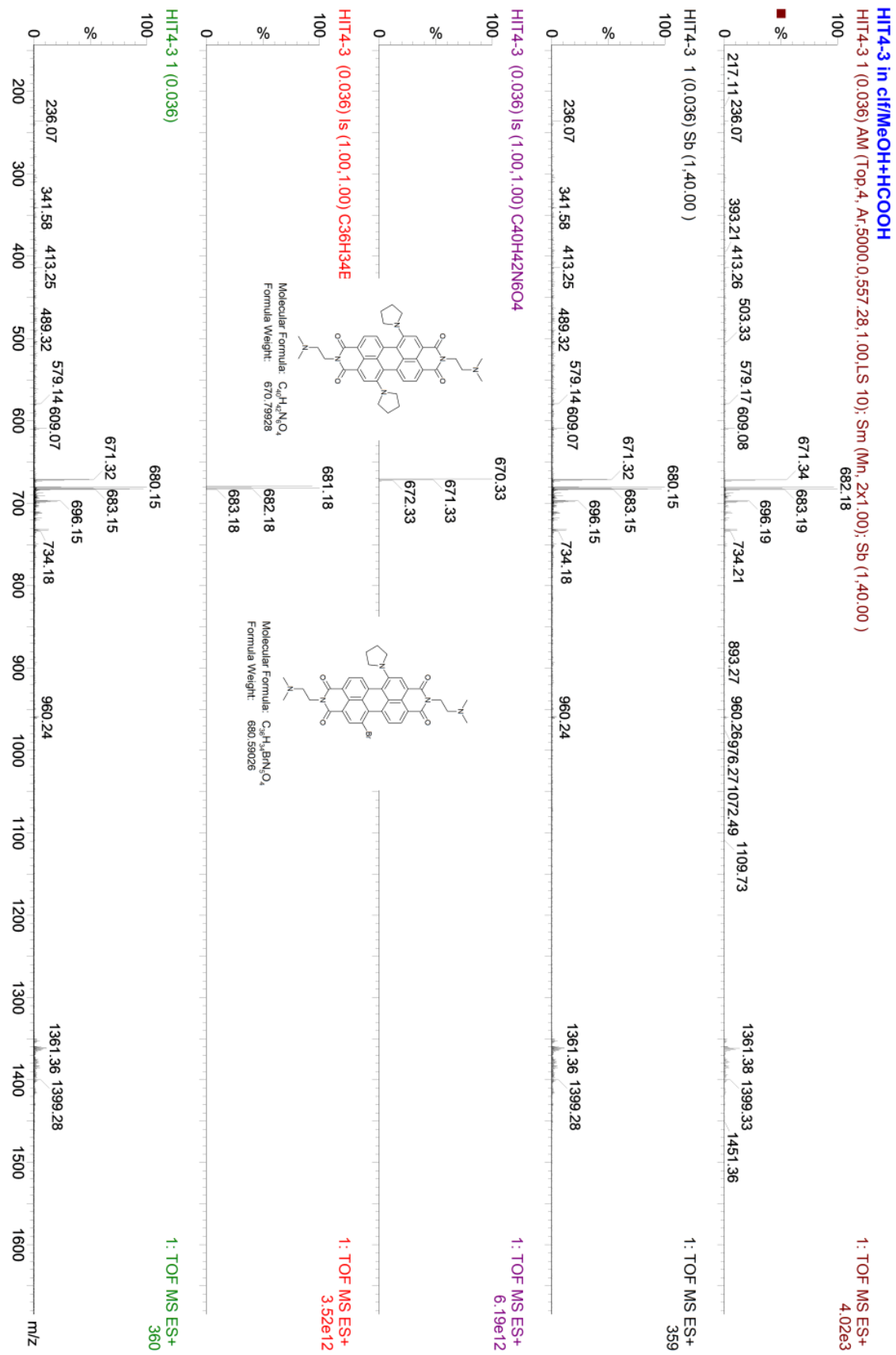

Figure 41. *MS (ESI-TOF) results from second attempt on monopyrrolidine substitution.*

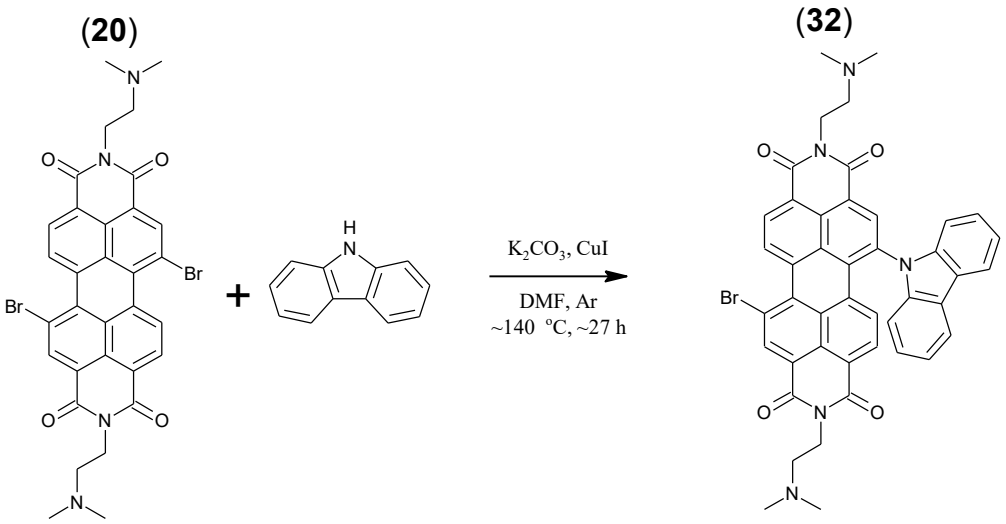

Figure 42. *First attempt on mono9H-carbazole substitution.*

Mono 9H-carbazole substitution was attempted following the previous pyrrolidine reactions. Reaction was completed and CC was performed on product. 3 separate bands were collected, but no MS (ESI-TOF) results were obtained. This was due to extremely low amount of collected products and defective measurement equipment.

Second attempt was performed using scheme from below Figure 43. Same scheme was performed 4 times in total using different equalities. Equalities for 9H-carbazole were measured against component 20 and ranged from 0.65 to 3. All other components were equalized accordingly following procedure from literature. [56]

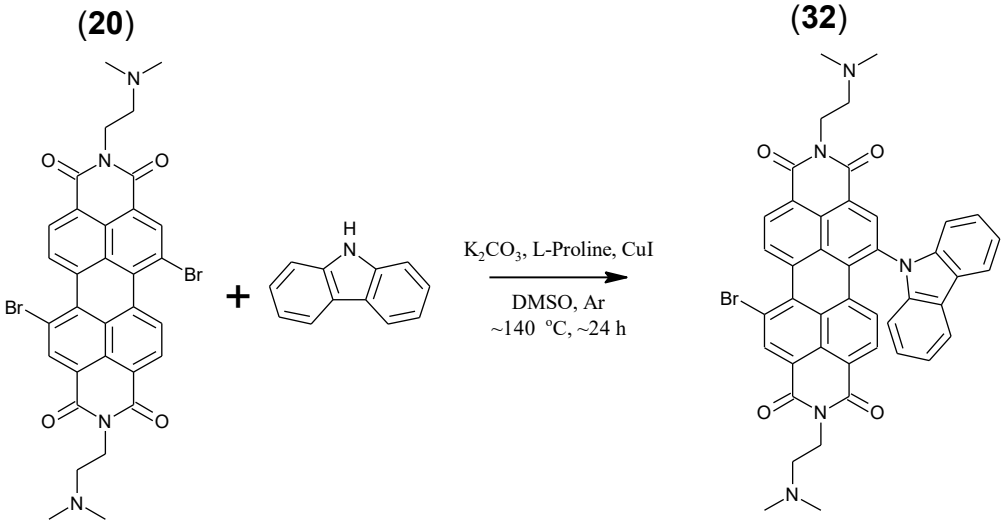

Figure 43. *Second attempt on mono 9H-carbazole substitution.*

However all of these attempts failed. Later it was discovered that K_2CO_3 was not completely dry. Unfortunately no additional attempts could be performed due to lack of time.

3.4 Following work

This dye was created as a candidate for ROS production. Subsequent actions should aim for proving the antimicrobial abilities of this dye. This could be performed simply by dissolving small amount of dye to water and applying this colored water to filter paper. This should create sufficient matrix for the dye. Although leeching will be an issue, this setup should provide comparable results in efficacy of this dye. In addition this test setup could be applied to verify the dark toxicity of this perylene diimide dye against selected bacteria. Furthermore its singlet oxygen generating ability should be tested.

4. EXPERIMENTAL

All commercially available solvents and reagents were purchased from Sigma-Aldrich or from VWR (Merck KGaA) and were used without further purification unless otherwise mentioned. All reactions were done using magnetic stirring unless stated otherwise. Reaction vessels were 40 ml clear glass vials made by VWR with screw necks. [57] Purification of products was performed by column chromatography or by preparative thin layer chromatography (TLC) plates. In CC the column was prepared using silica 100 (Merck) with pore size 0.063-0.200 mm. TLC plates were coated with aluminum oxide 60 F_{254} (Merck). Water refers to purified Milli-Q® water.

High-resolution mass spectra were recorded using Waters LTC Premier XE ESI-TOF bench top mass spectrometer. Leucine enkephaline (LEU-ENK) was used as reference compound in acquisition of mass. Nuclear magnetic resonance spectra were recorded using a 300 MHZ Varian Mercury spectrometer using TMS as internal standard. Absorption spectra were measured using Shimadzu UV-2510PC UV-Vis Recording spectrometer.

Glass filters were produced by Duran and their nominal pore sizes are in the Table 3 below. [58]

Table 3. *Porosity table. Porosity number in left column and nominal pore size in right column.*

Porosity	Nominal max. pore size (µm)
0	160-250
1	100-160
2	40-100
3	16-40
4	10-16
5	1.0-1.6

4.1 Synthesis

Synthesis of 5,12-dibromoisochromeno[4',5',6':6,5,10]anthra[2,1,9-def]isochromene-1,3,8,10-tetrone (18)

Synthesis was done accordimg to the procedure from literature. [59] A total of 0.9992 g (1.311 mmol) of PTCDA was dissolved in 8.3 ml of concentrated H_2SO_4 and solution was stirred in RT for approximately 24 hours to dissolve PTCDA. 0.0358 g (0.077 mmol) of I_2 was added and after 20 minutes 0.15 ml (2.919 mmol) of Br_2 was added. Reaction was heated to 90 °C for approximately 24 hours while stirring. Excess bromine was let out of reaction vessel by air flow. Water was added to reaction vessel to precipitate product. Product was first washed with 86 % H_2SO_4 solution and then with water until the pH of waste water reached neutral level. Washing of product was done in №4 filter with applied suction. Product was placed in to vacuum desiccator to remove water.

Synthesis of 5,12-dibromo-2,9-bis[2-(dimethylamino)ethyl]isoquinolino[4',5',6':6,5,10]anthra[2,1,9-def]isoquinoline-1,3,8,10(2H,9H)-tetrone (19)

Synthesis was done following a procedure mentioned in the literature. [60] A total of 0.4117 g (0.748 mmol) of dibromo PTCDA was dissolved in mixture of 4.3 ml of dioxane and 6.3 ml of dimethylformamide (DMF) under Ar-atmosphere in RT while stirring. 0.18 ml (1.672 mmol) of N,N-dimethylethane-1,2-diamine was added under Ar-atmosphere and heating was starter. Reaction was heated to 90-100 °C for 2 hours while stirring. Mixture was cooled to RT and water was added to precipitate the product. Product was filtered on filtered on №4 filter and washed with water several times. Product was purified with column chromatography using around 50 ml of silica 100 with $CHCl_3$:EtOH:Et_3N (93:6.5:0.5) as eluent. Product was red solid 0.3425 g with 66% yield. **Dibromo PDI** ^{1}H NMR (300 MHz,$CDCl_3$) δ ppm 2.31 - 2.40 (m, 13 H) 2.64 - 2.73 (m, 4 H) 4.30 - 4.41 (m, 4 H) 8.57 - 8.65 (m, 2 H) 8.81 - 8.87 (m, 2 H) 9.38 (d, *J*=8.19 Hz, 2 H). ESI-TOF (ES+, in $CHCl_3$/MeOH 10:15) m/z calcd. for $C_{32}H_{27}Br_2N_4O_4$ [M+H] 691.0381, found 691.0353.

Synthesis of 2,9-bis[2-(dimethylamino)ethyl]-5,12-bis(pyridin-4-ylsulfanyl)isoquinolino[4',5',6':6,5,10]anthra[2,1,9-def]isoquinoline-1,3,8,10(2H,9H)-tetrone (20)

A total of 0.0498 g, (0.072 mmol) of compound 2 was placed in a 40 ml vial under Ar-atmosphere in RT. 0.0246 g (0.178 mmol) of dry K_2CO_3 was added to vial. As solvent 4.1 ml of 1-Methylpyrrolidin-2-one (NMP) was added to vial. Then 0.0243 g (0.219 mmol) of Pyridine-4-thiol was added and vial was placed under cooling. Reaction was cooled between -10 °C and -5 °C and kept there for 3 hours. Reaction was stopped by adding water. Product was dissolved in $CHCl_3$ and washed with water several times. Excess solvent was removed and product was purified by aluminum oxide plates using $CHCl_3$:EtOH (100:1) as eluent giving 0.0394 g, 72.8 % of violet solid as yield. **Dimercaptopyridine PDI** ^{1}H NMR (300 MHz, CHLOROFORM-*d*) δ ppm 2.36 (s, 12 H) 2.70

(t, *J*=6.73 Hz, 4 H) 4.34 (t, *J*=6.73 Hz, 4 H) 7.05 - 7.20 (m, 4 H) 8.48 (dd, *J*=4.39, 1.46 Hz, 4 H) 8.64 - 8.78 (m, 4 H) 8.86 (d, *J*=8.19 Hz, 2 H). ESI-TOF (ES+, in $CHCl_3$/MeOH 10:15) m/z calcd. for $C_{42}H_{34}N_6O_4S_2$ [M] 751.2161, found 751.2141. Abs λ_{max} (ε, $M^{-1}cm^{-1}$ in H_2O) 533 (16019).

Synthesis of 4,4'-({1,3,8,10-tetraoxo-2,9-bis[2-(trimethylammonio)ethyl]-1,2,3,8,9,10-hexahydroisoquinolino[4',5',6':6,5,10]anthra[2,1,9-def]isoquinoline-5,12-diyl}disulfanediyl)bis(1-methylpyridinium) tetraiodide (21)

A total of 0.0153 g (0.027 mmol) of compound 3 was added in to vial. Then 0.5 ml (8.032 mmol) of MeI was added to vial with 3.0 ml of DMF acting as solvent. Vial was kept in RT and stirring for around 16 hours. After this product was precipitated and washed with diethyl ether several times to remove excess MeI and DMF. Product was dark red/violet solid 0.0264 g, 74.2 % yield. **QtSalt of dimercaptopyridine PDI** ^{1}H NMR (300 MHz, DEUTERIUM OXIDE) δ ppm 3.31 (s, 18 H) 3.67 - 3.78 (m, 4 H) 4.04 (s, 6 H) 4.58 - 4.67 (m, 4 H) 7.52 (d, *J*=6.44 Hz, 4 H) 8.25 (d, *J*=7.02 Hz, 4 H) 8.42 (d, *J*=8.19 Hz, 2H) 8.60 (s, 2 H) 8.69 (d, *J*=8.19 Hz, 2 H). ESI-TOF (ES+, in CH_3CN/H_2O 4:1) m/z calcd. for $C_{46}H_{46}N_6O_4S_2$ $[M\text{-}4I]^{4+}$ 202.5755, found 202.5741; calcd. for $C_{46}H_{46}N_6O_4S_2$ $[M+Me]^{3+}$ 270.1007, found 270.0973;calcd. for $C_{46}H_{46}IN_6O_4S_2$ $[M\text{-}3I]^{3+}$ 312.4022, found 312.4009; calcd. for $C_{46}H_{46}I_2N_6O_4S_2$ $[M\text{-}2I]^{2+}$ 532.0556, found 532.0536. Abs λ_{max} (ε, $M^{-1}cm^{-1}$ in H_2O) 530 (24344)

5. CONCLUSIONS

Novel perylene diimide dye was synthesized and characterized by NMR, MS and UV-Vis. spectral data confirmed the supposed structure.

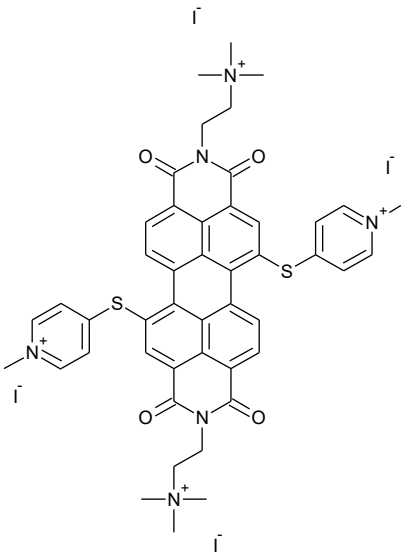

Figure 44. *Structure of novel perylene derivative dye. Dye is in cationic form.*

Synthetic scheme is presented in **45** below.

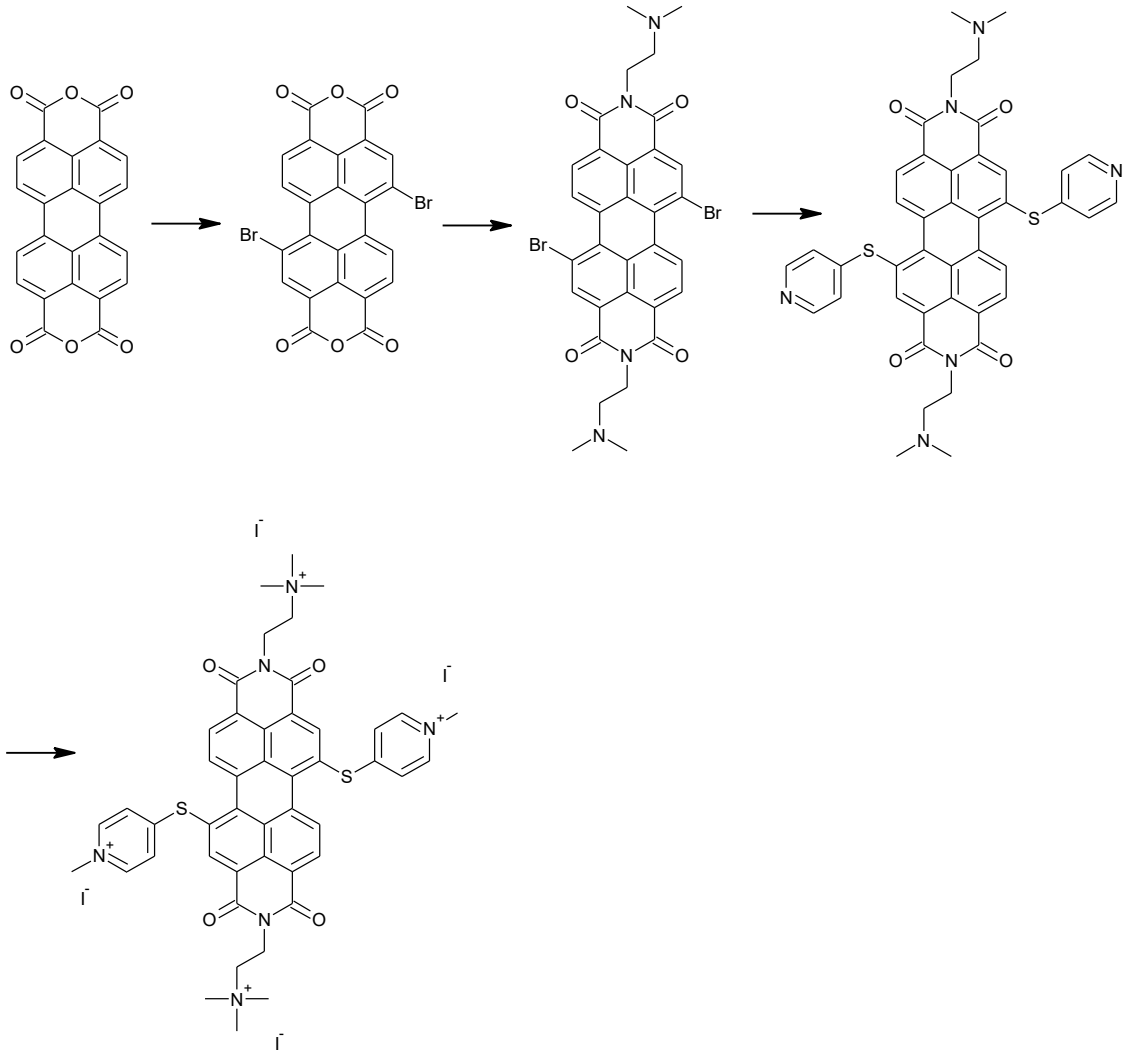

Figure 45. *Synthetic scheme for perylene diimide derivate dye.*

REFERENCES

[1] M. Wainwright, "In defence of 'dye therapy,'" *Int. J. Antimicrob. Agents*, vol. 44, no. 1, pp. 26–29, 2014.

[2] R. M. Donlan and J. W. Costerton, "Biofilms: survivalmechanisms of clinically relevant microorganisms.," *Clin.Microbiol. Rev.*, vol. 15, no. 2, pp. 167–19, 2002.

[3] WHO, "Antimicrobial resistance. Global Report on Surveillance," *Bull. World Health Organ.*, vol. 61, no. 3, pp. 383–94, 2014.

[4] H. W. Boucher *et al.*, "Bad Bugs, No Drugs: No ESKAPE! An Update from the Infectious Diseases Society of America," *Clin. Infect. Dis.*, vol. 48, no. 1, pp. 1–12, 2009.

[5] F. Vatansever *et al.*, "Antimicrobial strategies centered around reactive oxygen species - bactericidal antibiotics, photodynamic therapy, and beyond," *FEMS Microbiol. Rev.*, vol. 37, no. 6, pp. 955–989, 2013.

[6] M. Tim, "Strategies to optimize photosensitizers for photodynamic inactivation of bacteria," *J. Photochem. Photobiol. B Biol.*, vol. 150, pp. 2–10, 2015.

[7] S. S. Zumdahl, *Chemical Principles Sixth Edition*. .

[8] D. B. Min and J. M. Boff, "Chemistry and Reaction of Singlet Oxygen in Foods," *Compr. Rev. Food Sci. Food Saf.*, vol. 1, no. 2, pp. 58–72, 2002.

[9] K. P. Jensen and U. Ryde, "How O2 binds to heme. Reasons for rapid binding and spin inversion," *J. Biol. Chem.*, 2004.

[10] E. Choe and D. B. Min, "Mechanisms and factors for edible oil oxidation," *Compr. Rev. Food Sci. Food Saf.*, vol. 5, no. 4, pp. 169–186, 2006.

[11] M. C. DeRosa and R. J. Crutchley, "Photosensitized singlet oxygen and its applications," *Coord. Chem. Rev.*, vol. 233–234, pp. 351–371, 2002.

[12] D. R. Kearns, "Physical and chemical properties of singlet molecular oxygen," *Chem. Rev.*, vol. 71, no. 4, pp. 395–427, Aug. 1971.

[13] A. R. Lang, *Dyes and Pigments: New Research*. 2009.

[14] L. M. Baltazar, A. Ray, D. A. Santos, P. S. Cisalpino, A. J. Friedman, and J. D. Nosanchuk, "Antimicrobial photodynamic therapy: An effective alternative approach to control fungal infections," *Front. Microbiol.*, vol. 6, no. MAR, pp. 1–11, 2015.

[15] F. Wilkinson, W. P. Helman, and A. B. Ross, "Quantum Yields for the Photosensitized Formation of the Lowest Electronically Excited Singlet State of Molecular Oxygen in Solution," *J. Phys. Chem. Ref. Data*, vol. 22, no. 1, pp. 113–

262, Jan. 1993.

[16] A. Telfer, S. M. Bishop, D. Phillips, and J. Barber, “Isolated photosynthetic reaction center of photosystem II as a sensitizer for the formation of singlet oxygen: Detection and quantum yield determination using a chemical trapping technique,” *J. Biol. Chem.*, vol. 269, no. 18, pp. 13244–13253, 1994.

[17] E. L. Clennan, “New Mechanistic and Synthetic Aspects of Singlet Oxygen Chemistry,” *Tetrahedron*, vol. 56, no. 47, pp. 9151–9179, Nov. 2000.

[18] N. Hoffmann, “Photochemical reactions as key steps in organic synthesis,” *Chem. Rev.*, vol. 108, no. 3, pp. 1052–1103, 2008.

[19] A. B. Ormond and H. S. Freeman, “Dye sensitizers for photodynamic therapy,” *Materials (Basel).*, vol. 6, no. 3, pp. 817–840, 2013.

[20] A. Krieger-Liszkay, C. Fufezan, and A. Trebst, “Singlet oxygen production in photosystem II and related protection mechanism,” *Photosynth. Res.*, vol. 98, no. 1–3, pp. 551–564, 2008.

[21] T. Dahl, W. RobertMiddenand, and P. Hartman, “PURE SINGLET OXYGEN CYTOTOXICITY FOR BACTERIA,” *Photochem. Photobiol.*, vol. 46, no. 3, pp. 345–352, Sep. 1987.

[22] T. Dahl, W. R. Midden, and D. C. Neckers, “COMPARISON OF PHOTODYNAMIC ACTION BY ROSE BENGAL IN GRAM-POSITIVE AND GRAM-NEGATIVE BACTERIA,” *Photochem. Photobiol.*, vol. 48, no. 5, pp. 607–612, Nov. 1988.

[23] J. A. Otter, S. Yezli, J. A. G. Salkeld, and G. L. French, “Evidence that contaminated surfaces contribute to the transmission of hospital pathogens and an overview of strategies to address contaminated surfaces in hospital settings,” *Am. J. Infect. Control*, vol. 41, no. 5 SUPPL., pp. S6–S11, 2013.

[24] C. Spagnul, L. C. Turner, and R. W. Boyle, “Immobilized photosensitizers for antimicrobial applications,” *J. Photochem. Photobiol. B Biol.*, vol. 150, pp. 11–30, 2015.

[25] R. Cahan, R. Schwartz, Y. Langzam, and Y. Nitzan, “Light-activated antibacterial surfaces comprise photosensitizers,” *Photochem. Photobiol.*, vol. 87, no. 6, pp. 1379–1386, 2011.

[26] J. Johnson Inbaraj, M. V. Vinodu, R. Gandhidasan, R. Murugesan, and M. Padmanabhan, “Photosensitizing properties of ionic porphyrins immobilized on functionalized solid polystyrene support,” *J. Appl. Polym. Sci.*, vol. 89, no. 14, pp. 3925–3930, 2003.

[27] C. Piccirillo *et al.*, “Antimicrobial activity of methylene blue and toluidine blue O covalently bound to a modified silicone polymer surface,” *J. Mater. Chem.*, vol. 19, no. 34, p. 6167, 2009.

[28] J. Bozja, J. Sherrill, S. Michielsen, and I. Stojiljkovic, “Porphyrin-based, light-

activated antimicrobial materials," *J. Polym. Sci. Part A Polym. Chem.*, vol. 41, no. 15, pp. 2297–2303, 2003.

[29] J. Sherrill, S. Michielsen, and I. Stojiljkovic, "Grafting of light-activated antimicrobial materials to nylon films," *J. Polym. Sci. Part A Polym. Chem.*, vol. 41, no. 1, pp. 41–47, 2002.

[30] R. R. Allison, G. H. Downie, R. Cuenca, X. H. Hu, C. J. H. Childs, and C. H. Sibata, "Photosensitizers in clinical PDT," *Photodiagnosis Photodyn. Ther.*, vol. 1, no. 1, pp. 27–42, 2004.

[31] E. D. Sternberg, D. Dolphin, and C. Brückner, "Porphyrin-based photosensitizers for use in photodynamic therapy," *Tetrahedron*, vol. 54, no. 17, pp. 4151–4202, 1998.

[32] R. Bonnett, "E l 4NS, U. K.," 1987.

[33] R. Bonnett, P. Charlesworth, B. D. Djelal, S. Foley, D. J. Mcgarvey, and T. G. Truscott, "porphyrin (m-THPP), 5 , 10 , 15 , 20-tetrakis (m-hydroxyphenyl) chlorin chlorin (m-THPBC): a comparative study," *In Vivo (Brooklyn).*, pp. 325–328, 1999.

[34] N. Masilela, P. Kleyi, Z. Tshentu, G. Priniotakis, P. Westbroek, and T. Nyokong, "Photodynamic inactivation of Staphylococcus aureus using low symmetrically substituted phthalocyanines supported on a polystyrene polymer fiber," *Dye. Pigment.*, vol. 96, no. 2, pp. 500–508, 2013.

[35] M. Wainwright, "The development of phenothiazinium photosensitisers," *Photodiagnosis Photodyn. Ther.*, vol. 2, no. 4, pp. 263–272, 2005.

[36] T. Kiesslich, A. Gollmer, T. Maisch, M. Berneburg, and K. Plaetzer, "A comprehensive tutorial on in vitro characterization of new photosensitizers for photodynamic antitumor therapy and photodynamic inactivation of microorganisms," *Biomed Res. Int.*, vol. 2013, 2013.

[37] A. Gollmer, A. Felgenträger, W. Bäumler, T. Maisch, and A. Späth, "A novel set of symmetric methylene blue derivatives exhibits effective bacteria photokilling - a structure-response study.," *Photochem. Photobiol. Sci.*, vol. 14, no. 2, pp. 335–351, 2015.

[38] S. A. and K. Z. Soheil Zorofchian Moghadamtousi, Habsah Abdul Kadir, Pouya Hassandarvish, Hassan Tajik, "A Review on Antibacterial, Antiviral, and Antifungal Activity of Curcumin.," *Biomed Res Int*, vol. 2014, 2014.

[39] A. Shrestha and A. Kishen, "Polycationic Chitosan-Conjugated Photosensitizer for Antibacterial Photodynamic Therapy†," *Photochem. Photobiol.*, vol. 88, no. 3, pp. 577–583, May 2012.

[40] W. Lei, Q. Zhou, G. Jiang, B. Zhang, and X. Wang, "Photodynamic inactivation of Escherichia coli by Ru(ii) complexes," *Photochem. Photobiol. Sci.*, vol. 10, no. 6, p. 887, 2011.

[41] P. Parakh, S. Gokulakrishnan, and H. Prakash, “Visible light water disinfection using [Ru(bpy)2(phendione)] (PF6)2??2H2O and [Ru(phendione) 3]Cl2??2H2O complexes and their effective adsorption onto activated carbon,” *Sep. Purif. Technol.*, vol. 109, pp. 9–17, 2013.

[42] C. C. Chao *et al.*, “Photophysical and electrochemical properties of 1,7-diaryl-substituted perylene diimides,” *J. Org. Chem.*, vol. 70, no. 11, pp. 4323–4331, 2005.

[43] H. Dinçalp, Ş. Kizilok, and S. Içli, “Fluorescent macromolecular perylene diimides containing pyrene or indole units in bay positions,” *Dye. Pigment.*, vol. 86, no. 1, pp. 32–41, 2010.

[44] C. Li *et al.*, “Rainbow perylene monoimides: Easy control of optical properties,” *Chem. - A Eur. J.*, vol. 15, no. 4, pp. 878–884, 2009.

[45] S. M. Kerwin, G. Chen, J. T. Kern, and P. W. Thomas, “Perylene diimide G-quadruplex DNA binding selectivity is mediated by ligand aggregation,” *Bioorganic Med. Chem. Lett.*, vol. 12, no. 3, pp. 447–450, 2002.

[46] O. Y. Fedoroff, M. Salazar, H. Han, V. V. Chemeris, S. M. Kerwin, and L. H. Hurley, “NMR-based model of a telomerase-inhibiting compound bound to G-quadruplex DNA,” *Biochemistry*, vol. 37, no. 36, pp. 12367–12374, 1998.

[47] H. Dinçalp, Ş. KIzIlok, and S. Içli, “Targeted singlet oxygen generation using different DNA-interacting perylene diimide type photosensitizers,” *J. Fluoresc.*, vol. 24, no. 3, pp. 917–924, 2014.

[48] Y. Shieh, S. Yang, M. Wei, and M. Shieh, “Aptamer-Based Tumor-Targeted Drug,” vol. 4, no. 3, pp. 1433–1442, 2010.

[49] T. Kircher and H. G. Lohmannsroben, “Photoinduced charge recombination reactions of a perylene dye in acetonitrile,” *Phys. Chem. Chem. Phys.*, vol. 1, no. 17, pp. 3987–3992, 1999.

[50] C. Huang, S. Barlow, and S. R. Marder, “Perylene-3,4,9,10-tetracarboxylic acid diimides: Synthesis, physical properties, and use in organic electronics,” *J. Org. Chem.*, vol. 76, no. 8, pp. 2386–2407, 2011.

[51] Y. Nagao, “Synthesis and properties of perylene pigments,” *Prog. Org. Coatings*, vol. 31, no. 1–2, pp. 43–49, 1997.

[52] L. M. Wangatia, B. Sun, T. Zeng, and M. Zhu, “Reactive bay functionalized perylene monoimide-polyhedral oligomeric silsesquioxane organic electronic dye,” *Mater. Sci. Pol.*, vol. 33, no. 1, pp. 113–121, 2015.

[53] M. Bagui *et al.*, “Synthesis and optical properties of perylene diimide derivatives with triphenylene-based dendrons linked at the bay positions through a conjugated ethynyl linkage,” *Tetrahedron*, vol. 68, no. 13, pp. 2806–2818, 2012.

[54] Á. J. Jiménez *et al.*, “A tightly coupled bis(zinc(ll) phthalocyanine)-perylenediimide ensemble to yield long-lived radical ion pair states,” *Org. Lett.*,

vol. 9, no. 13, pp. 2481–2484, 2007.

[55] G. R. Fulmer *et al.*, "NMR chemical shifts of trace impurities: Common laboratory solvents, organics, and gases in deuterated solvents relevant to the organometallic chemist," *Organometallics*, vol. 29, no. 9, pp. 2176–2179, 2010.

[56] W.-Y. Lai, Q.-Y. He, D.-Y. Chen, and W. Huang, "Synthesis and Characterization of Starburst 9-Phenylcarbazole/Triazatruxene Hybrids," *Chem. Lett.*, vol. 37, no. 9, pp. 986–987, Sep. 2008.

[57] "Certificate of Conformity VWR EPA SCREW NECK VIALS ND24," no. April 2012, p. 3001.

[58] DWK Life Sciences, "Duran - Glass filtration apparatus and accessories," 2017. [Online]. Available: http://www.duran-group.com/en/products-solutions/laboratory-glassware/products/glass-filtration-apparatus-and-accessories/filter-funnel.html. [Accessed: 06-Oct-2017].

[59] F. Wu, V. Stepanenko, Z. Chen, C. R. Saha-mo, N. Kocher, and D. Stalke, "Preparation and Characterization of Regioisomerically Pure 1 , 7-Disubstituted Perylene Bisimide Dyes," *J. Org. Chem.*, vol. 69, no. 11, pp. 7933–7939, 2004.

[60] A. Weißenstein and F. Würthner, "Metal ion templated self-assembly of crown ether functionalized perylene bisimide dyes," *Chem. Commun.*, vol. 51, no. 16, pp. 3415–3418, 2015.

APPENDIX A: SYNTHETIC PLANS

Synthesis of perylenemides for singlet oxygen generation

Plan 1

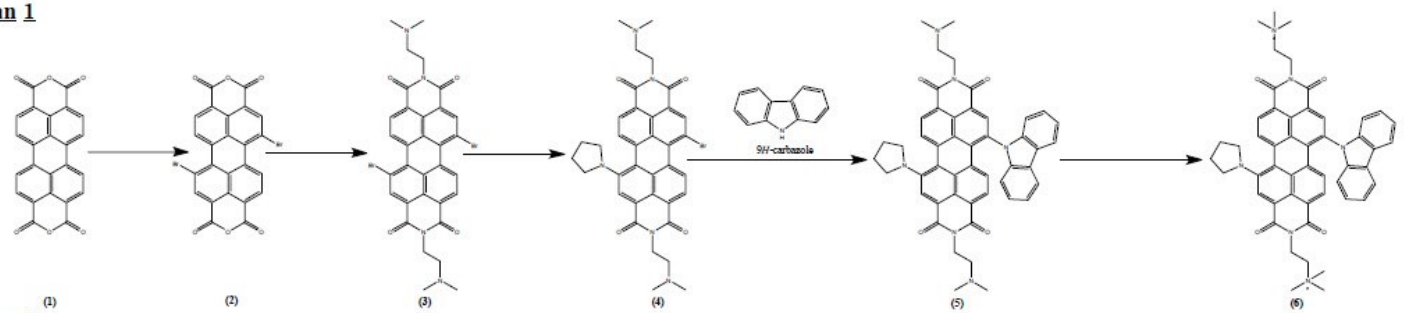

Plan 2

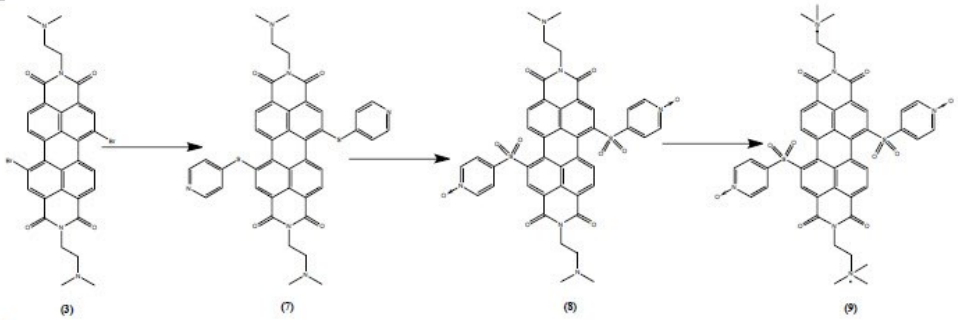

Plan 3

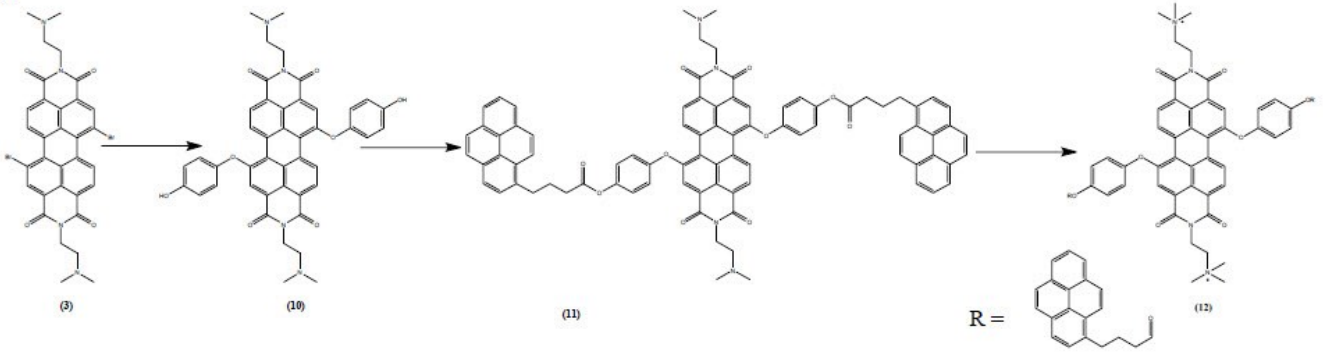

APPENDIX B: MS (ESI-TOF) ON DIBROMO PDI

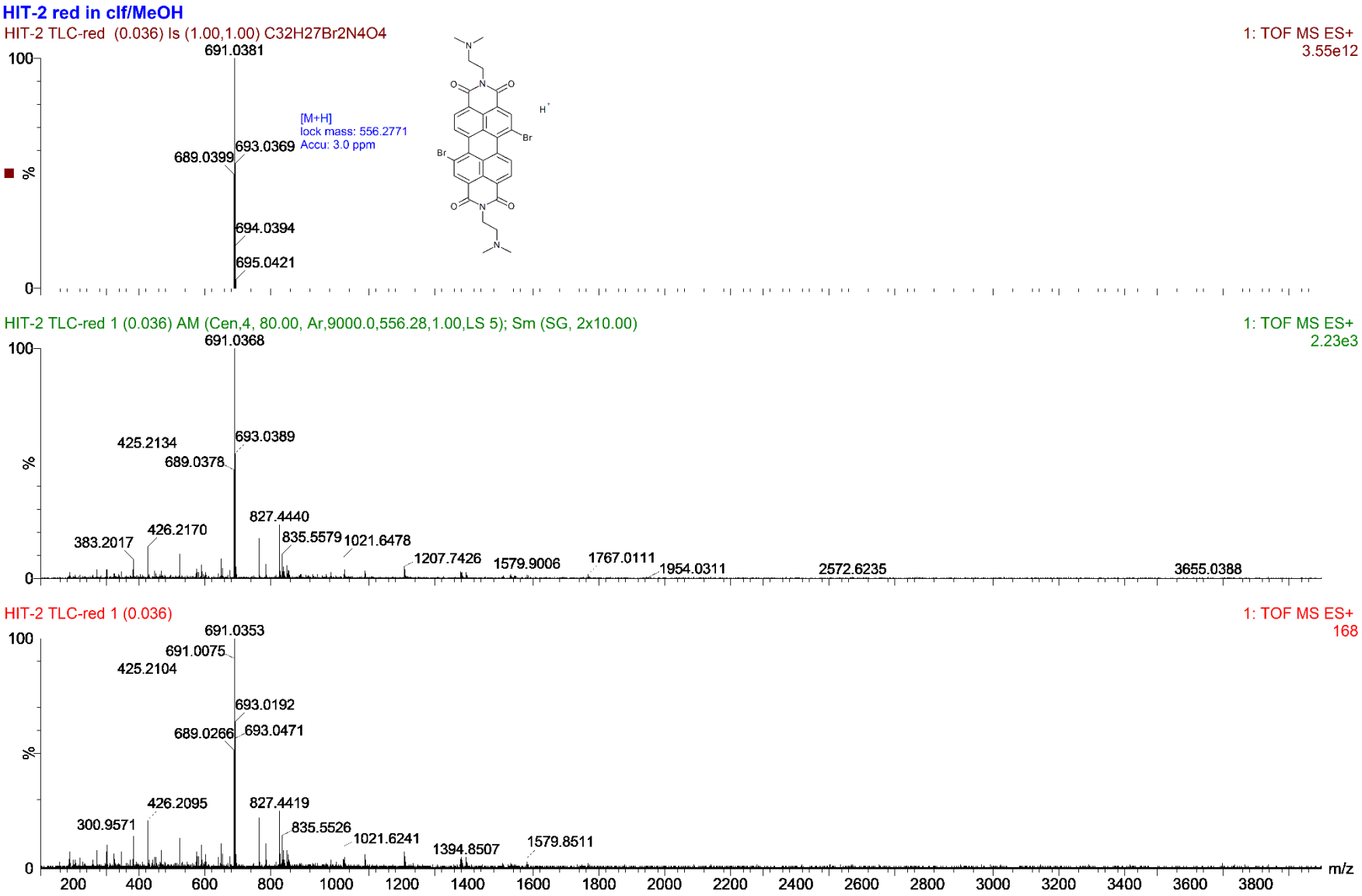

APPENDIX C: MS (ESI-TOF) ON DIMERCAPTO-PYRIDINE PDI

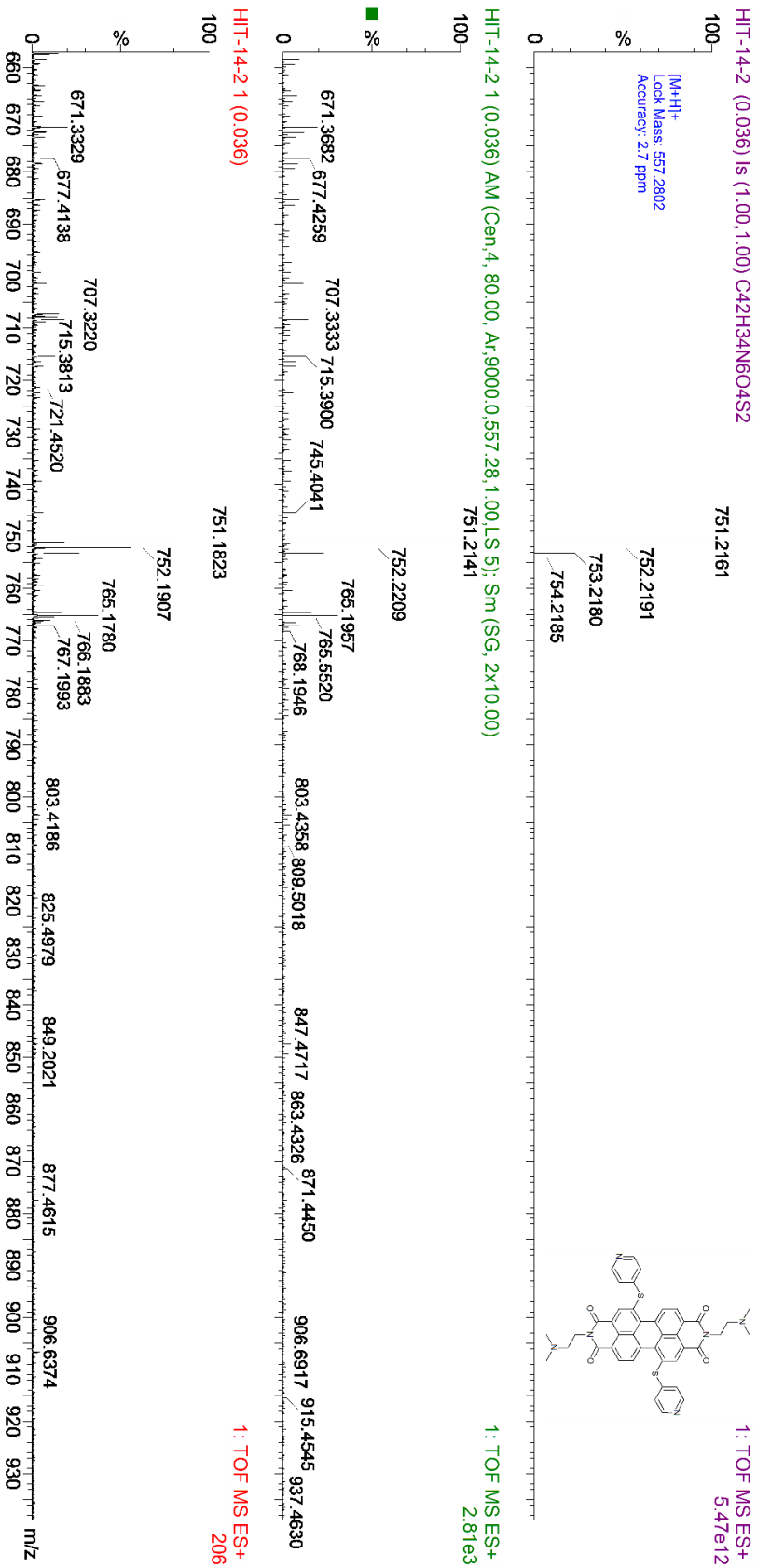

APPENDIX D: MS (ESI-TOF) ON QT-SALT OF DI-MERCAPTOPYRIDINE PDI